HHS Public Access

Author manuscript

Sci Signal. Author manuscript; available in PMC 2020 December 24.

Published in final edited form as:

Sci Signal. ; 12(569): . doi:10.1126/scisignal.aat8595.

Disabling the Gβγ-SNARE interaction disrupts GPCR-mediated presynaptic inhibition, leading to physiological and behavioral phenotypes

Zack Zurawski[1,2], **Analisa D. Thompson Gray**[1], **Lillian J. Brady**[1], **Brian Page**[2], **Emily Church**[2], **Nicholas A. Harris**[3], **Michael R. Dohn**[1], **Yun Young Yim**[1], **Karren Hyde**[1], **Douglas P. Mortlock**[3], **Carrie K. Jones**[1,4], **Danny G. Winder**[3], **Simon Alford**[2], **Heidi E. Hamm**[1,*]

[1]Department of Pharmacology, Vanderbilt University, Nashville, TN 37232, USA.

[2]Department of Anatomy and Cell Biology, University of Illinois at Chicago, Chicago, IL 60612, USA.

[3]Department of Molecular Physiology and Biophysics, Vanderbilt University, Nashville, TN 37232, USA.

[4]Vanderbilt Center for Neuroscience Drug Discovery, Vanderbilt University, Nashville, TN 37232, USA.

Abstract

G protein–coupled receptors (GPCRs) that couple to $G_{i/o}$ proteins modulate neurotransmission presynaptically by inhibiting exocytosis. Release of Gβγ subunits from activated G proteins decreases the activity of voltage-gated Ca^{2+} channels (VGCCs), decreasing excitability. A less understood Gβγ−mediated mechanism downstream of Ca^{2+} entry is the binding of Gβγ to SNARE complexes, which facilitate the fusion of vesicles with the cell plasma membrane in exocytosis. Here, we generated mice expressing a form of the SNARE protein SNAP25 with premature truncation of the C terminus and that were therefore partially deficient in this interaction. SNAP25Δ3 homozygote mice exhibited normal presynaptic inhibition by $GABA_B$ receptors, which inhibit VGCCs, but defective presynaptic inhibition by receptors that work directly on the SNARE complex, such as 5-hydroxytryptamine (serotonin) $5\text{-}HT_{1b}$ receptors and adrenergic α_{2a} receptors. Simultaneously stimulating receptors that act through both mechanisms showed synergistic inhibitory effects. SNAP25Δ3 homozygote mice had various behavioral phenotypes, including increased stress-induced hyperthermia, defective spatial learning, impaired gait, and supraspinal nociception. These data suggest that the inhibition of exocytosis by $G_{i/o}$-

*Corresponding author. heidi.hamm@vanderbilt.edu.

Author contributions: Z.Z., D.P.M., D.G.W., S.A., C.K.J., and H.E.H. conceived the project and experiments. Z.Z., A.D.T.G., L.J.B., Y.Y.Y., N.A.H., and S.A performed data analysis. Z.Z., A.D.T.G., Y.Y.Y., D.G.W., S.A., C.K.J., and H.E.H developed methodology. Z.Z., A.D.T.G., L.J.B., B.P., E.C., N.A.H., M.R.D., Y.Y.Y., and S. A conducted the experiments described within. Z.Z., A.D.T.G., L.J.B., N.A.H., Y.Y.Y., D.G.W., S.A., C.K.J., and H.E.H wrote the original draft of the manuscript. Z.Z., A.D.T.G., L.J.B., N.A.H., Y.Y.Y., D.G.W., S.A., C.K.J., and H.E.H reviewed and edited the manuscript. Z.Z., A.D.T.G., K.H., L.J.B., and D.P.M developed reagents and bred animals. H.E.H provided research funding. D.G.W., S.A., C.K.J., and H.E.H supervised the experiments.

Competing interests: The authors declare that they have no competing interests.

Data and materials availability: The SNAP25Δ3 mice require a materials transfer agreement from Vanderbilt University. All data needed to evaluate the conclusions in the paper are present in the paper or the Supplementary Materials.

coupled GPCRs through the Gβγ-SNARE interaction is a crucial component of numerous physiological and behavioral processes.

INTRODUCTION

G protein–coupled receptors (GPCRs) play a primary role in regulating every physiological function and every organ system. They modulate the secretion of hormones throughout the body. In the brain, GPCRs activated by neurotransmitters in turn modulate neurotransmission- and voltage-gated ion channels and are critical to the proper functioning of brain circuits, as well as their alterations in development, especially learning and memory. GPCR modulation occurs through many mechanisms, including second messengers and phosphorylation (1). In particular, $G_{i/o}$-coupled GPCRs inhibit secretion throughout the body through direct membrane-delimited action through Gβγ. In neurons, presynaptic modulation of neurotransmitter release is important in avoiding overstimulation by autoreceptors that inhibit the release of specific neurotransmitters, as well as for normal functioning of brain circuitry by heteroreceptors. $G_{i/o}$-coupled GPCRs inhibit exocytosis presynaptically through three main membrane-delimited mechanisms: by the voltage-dependent inhibition of calcium (Ca^{2+}) entry through the binding of Gβγ to voltage-gated Ca^{2+} channels (VGCCs) (2–10); by Gβγ-mediated activation of G protein–coupled inwardly-rectifying potassium (K^{+}) channels (11–13), leading to membrane hyperpolarization; and by direct interaction of Gβγ with the exocytotic apparatus, causing inhibition of exocytosis(14–29).

An accepted mechanism of presynaptic inhibition involves $G_{i/o}$-coupled GPCR modulation of Ca^{2+} entry at the active zone (10,30–33). Free cytosolic Ca^{2+} increases neurotransmitter release with a 4^{th} power non-linear relationship (34,35) between concentration and exocytosis, and inhibition of Ca^{2+} entry inhibits exocytosis. Direct Gβγ modulation of VGCC has been demonstrated at the presynaptic terminal with Ca^{2+}-sensitive dyes (25) and more directly, electrophysiologically at cell bodies and at the calyceal synapse of Held (36,37). $G_{i/o}$-coupled GPCRs also inhibit the frequency of spontaneous firing and Ca^{2+}-independent neurotransmitter release through less well-understood mechanisms (38–44). Direct inhibition of exocytotic fusion controls exocytosis linearly and does not require changes in diffusible cytoplasmic calcium. Gβγ modulates exocytotic fusion by binding the membrane-proximal C-terminal end of the soluble NSF attachment protein receptor (SNARE) complex that brings the vesicle close to the plasma membrane. We have shown that Botulinum Toxin Type-A (BoNT/A) functionally uncouples this direct Gβγ−SNARE interaction by cleaving the C-terminal 9aa from SNAP25; in addition, a peptide from this region can itself block presynaptic inhibition (17).

In biochemical support of the modulation at the exocytotic machinery, we have shown that Gβγ binds directly to ternary SNARE complexes, as well as to the target membrane-associated (t)-SNARE and the individual SNARE components SNAP25, syntaxin1A, and synaptobrevin 2/VAMP2, and competes with the binding of synaptotagmin I to t-SNARE and ternary SNARE complexes (16,21). In addition, we have shown that Gβγ inhibits exocytosis upon the activation of presynaptic Gi/o-coupled $5HT_{1B}$- like receptors (15,16,21,25). Modulatory effects of presynaptic GPCRs downstream of Ca^{2+} entry are

difficult to measure directly in the presynaptic terminal since this direct inhibition of exocytosis is invisible to Ca^{2+} imaging studies. Many critical questions remain unanswered about the importance of Gβγ regulation of the SNARE machinery in neuromodulation. For example, it is not known which $G_{i/o}$-GPCRs work by this mechanism. In particular, the relative importance of direct inhibition of release at the exocytotic apparatus compared to other $G_{i/o}$-GPCR evoked molecular events is unknown. Moreover, it is not known whether multiple Gβγ− dependent mechanisms operate synergistically. Finally, nothing is known about the importance of this mechanism in physiology in vivo and in producing fine-tuned behaviors.

To investigate the role of the Gβγ-SNARE interaction in normal physiology, we created a transgenic mouse deficient in this interaction using the CRISPR/Cas9 strategy. We focused on the SNAP25 target of Gβγ, because of the difficulty of removing Gβγ (5 Gβ's and 12 Gγ's), and because we do not know which of them is involved in interaction with the SNARE complex. Gβγ binds to the C-terminus of SNAP25, and we have determined that SNAP25Δ3 has a twofold reduction in Gβγ binding and a two-fold reduction in $5\text{-}HT_{1B}R$-mediated inhibition of exocytosis, while evoked release is normal (26,45). In the current study, we confirmed that C-terminally truncated t-SNARE complexes have a decreased ability to bind Gβγ and inhibit synaptotagmin 1-mediated liposome fusion in vitro. In vivo studies revealed that the SNAP25Δ3 mutant animals had behavioral and physiological defects in nociception and stress handling, motor coordination, affective behaviors, and cognitive behaviors linked to the central nervous system.

RESULTS

The SNAP25Δ3 mouse was generated using CRISPR-Cas9

To generate a mouse deficient in the Gβγ-SNARE interaction, we introduced the SNAP25Δ3 mutation into the eighth exon of *SNAP25* through the CRISPR/Cas9 interaction. We inserted the *SNAP25Δ3* allele into the wild-type (WT) *SNAP25* locus using CRISPR-Cas9 technology (Fig. 1A). PCR genotyping of B6D2 mouse pups transfected with the appropriate DNAs revealed three heterozygous mice that had undergone homology-directed repair out of 32 pups born (Fig. 1B). Heterozygous mice were fertile and were bred to C57BL6/J WT mice to yield homozygous offspring.

Homozygous offspring containing the SNAP25Δ3 mutation were viable at all developmental ages, and the general health, appearance, and breeding of these mutant mice was unremarkable relative to their age-matched littermate WT mice (Fig. 1C, left). SNAP25Δ3 mice also displayed normal growth curves relative to littermate WT mice, with comparable body weights from 3 to 60 weeks of age (Fig. 1C, right). Western blotting analysis showed that the abundances of a panel of synaptic proteins present in SNAP25Δ3 mouse brain homogenates were not different from those in the brains of WT animals, with the exception of cysteine string protein (CSP) (Fig. 1D, Supplemental Fig 1).

Gβγ interactions at presynaptic terminals are ubiquitous and loss of a site of interaction at the presynaptic terminal might cause neurodevelopmental defects. Thus, we used immunofluorescence microscopy to investigate potential differences in neuronal morphology

between adult WT and SNAP25Δ3 animals. Neuronal cell bodies were visualized with a mouse primary antibody against Hu protein isoformsC/D (46). Excitatory inputs onto observed soma were visualized with a primary antibody against the vesicular glutamate transporter isoform 2 (VGlut2), a marker of glutamatergic synapses, whereas inhibitory inputs were visualized with a primary antibody against the vesicular GABA transporter (VGAT), a marker of GABAergic synapses. No substantial differences were detected in the numbers of synaptic contacts, excitatory inputs, or inhibitory inputs between WT and SNAP25Δ3 littermates, supporting the notion that observed phenotypes are due to changes in neuronal signaling rather than changes in synaptic proteins or other gross morphological changes (Fig. 1E).

SNAP25Δ3 impairs Gβγ competition with synaptotagmin I and inhibition of Ca^{2+}-Synaptotagmin I–mediated liposome fusion

Gβγ mediates its effects on exocytosis through competition with the Ca^{2+} sensor synaptotagmin I (sytI) for interaction for the C-terminal region of SNAP25 (16,21). To investigate the in vitro phenotype of the SNAP25Δ3 mutation, we used total internal reflection (TIRF) microscopy (Fig. 2A, left panel) to determine whether recombinant Alexa Fluor (AF) 488–labeled sytI C2AB domains bound to membrane-associated WT and SNAP25Δ3 t-SNARE complexes differently in lipid membranes, and, to determine the potency with which purified bovine $G\beta_1\gamma_1$ competed with AF-sytI for binding sites on these mutant t-SNAREs. Gβγ competed with AF-sytI for binding sites on WT t-SNARE, causing a concentration-dependent reduction in both absolute fluorescence and anisotropy of the AF-sytI signal, with a half-maximal effect at 502 ± 151 nM (Fig. 2A, right panel). Substitution of SNAP25Δ3 into the t-SNARE in the lipid bilayer reduced the maximal effect of Gβγ on AF-sytI anisotropy to 47 ± 13 % of the WT effect (Fig. 2A, right). These data suggest that C-terminally truncated t-SNARE complexes have a decreased ability to bind to Gβγ.

Gβγ inhibit sytI- and SNARE-driven lipid mixing assays in a concentration-dependent manner (27). A more extensive C-terminal mutation of SNAP25, SNAP25Δ9, in which nine residues are truncated, displays reduced kinetics and a reduced maximal extent of lipid mixing compared to WT SNAP25 in lipid-mixing assays (47). Thus, we investigated whether the SNAP25Δ3 mutant behaved differently from WT SNAP25 in reconstituted vesicle fusion studies with SNARE complexes reconstituted into liposomes containing anionic phospholipids (47,48) (Fig. 2B). We observed no statistically significant difference between SNAP25Δ3 and WT SNAP25 with regards to the maximum extent of lipid mixing (Fig. 2C, left panel). The basal rate of lipid mixing in the absence of sytI C2AB was not statistically significantly different between SNAP25Δ3 and WT.

The reduced efficacy for Gβγ to displace Ca^{2+}-bound syt1 at SNARE complexes containing SNAP25Δ3 compared to complexes containing WT SNAP25 implies that the mutation modifies the ability of Gβγ to interfere with vesicle fusion. Indeed, $G\beta_1\gamma_1$ substantially inhibited lipid mixing at a concentration of 2 μM in liposomes containing t-SNAREs with WT SNAP25, but not SNAP25Δ3 (Fig. 2C). $G\beta_1\gamma_1$ inhibited lipid mixing substantially less well at a concentration of 6 μM in liposomes containing t-SNAREs with SNAP25Δ3 than in liposomes containing SNAP25 WT. We then performed pairwise comparisons between the

WT and the SNAP25Δ3 mutant t-SNAREs (Fig. 2C, right panel). Together, these data suggest that the SNAP25Δ3 mutant impairs Gβγ binding but has very little effect on lipid mixing or sytI C2AB function, which is consistent with a previous study (26).

SNAP25Δ3 mice have impaired sympathetic responses and loss of α_{2a}-adrenergic receptor function

Membrane delimited G protein mediated effects are ubiquitous at secretory cells and at presynaptic terminals. Gβγ modifies hormone secretion(24), and synaptic transmission in the peripheral and central nervous systems(5,6,15,19,28,49). However, these effects are mediated by more than one target of Gβγ including the SNARE complex. Thus, we next systematically characterized changes in the behavioral and/or physiological phenotypes of the SNAP25Δ3 homozygotes. Presynaptic inhibitory effects of GPCRs were first identified in the autonomic nervous system as autoreceptors controlling noradrenaline release(50). The presynaptic α_{2A}-adrenergic receptor (α_{2A}-AR) is $G_{i/o}$ –coupled and is known to work through the Gβγ-SNARE interaction. (19,24). If the inhibitory effects of α_{2A}-ARs are perturbed in the SNAP25Δ3 homozygotes, we might expect to see increased stress responses, because this receptor is the noradrenergic inhibitory autoreceptor that regulates the amount of norepinephrine (NE) release in the sympathetic system that controls fight and flight responses(51–53). To investigate whether the SNAP25Δ3 animals have exaggerated stress responses, we performed stress-induced hyperthermia studies in singly-housed age-matched littermate SNAP25Δ3 homozygotes and WT littermate controls(90). In the stress-induced hyperthermia paradigm(54), handling-based stress produces an increase in body temperature. Rectal temperatures were recorded before and after manual scruffing with an interval of 15min between each reading. SNAP25Δ3 homozygotes exhibited a twofold greater elevation in body temperature than WT littermates subsequent to handling (Fig. 3A). From this, we concluded that the SNAP25Δ3 mutation produces a stress hypersensitivity phenotype.

We next investigated the ability of the α_{2A}-AR to inhibit NE release as an autoreceptor(51,55) as well as glutamate release through heteroceptor mechanisms(56–58) (Fig. 3B) in age-matched littermate WT and mutant animals. To investigate the functions of α_{2A}-AR in the SNAP25Δ3 mice, we measured the effect of guanfacine, a partial α_{2A}-AR agonist, on excitatory glutamatergic transmission in the dorsal bed nucleus of the stria terminalis (dBNST). Guanfacine inhibits glutamate release in the BNST through a presynaptic mechanism(57), at least partially due to inhibition of parabrachial nucleus afferents in the region(58). Excitatory field potentials were recorded extracellularly as two negative deflections, the tetrodotoxin-sensitive fiber volley potential N1 and the AMPAR antagonist CNQX-sensitive synaptic potential N2(56) (Fig. 3C). As expected, bath application of guanfacine reduced N2 amplitude in WT mice, and the extent of this reduction was smaller in SNAP25Δ3 animals (Fig. 3D, 3E). To determine whether these effects were specific to the α_{2A}-AR or were translatable to other $G_{i/o}$-coupled GPCRs, we examined the effects of the $GABA_B$ agonist baclofen on excitatory transmission in the BNST. Bath application of 10 μM baclofen inhibited N2 amplitude in both WT and SNAP25Δ3 mice to a similar extent (Fig. 3F, 3G).

5-HT_{1b}- and Gβγ–SNARE–mediated inhibition of exocytosis are impaired in SNAP25Δ3 homozygotes, whereas $GABA_B$- and Gβγ–VGCC–mediated inhibition of exocytosis is normal

To understand the effect of disruption of the Gβγ-SNARE interaction on electrophysiological responses, we studied the $5HT_{1b}$-mediated inhibition of hippocampal CA1 to subiculum neurotransmission (Fig. 4A). The subiculum is an essential structure that receives the majority of its input from the hippocampus proper and projects to the entorhinal and other cortices, as well as to other subcortical regions. As such, the subiculum plays an important role in spatial and mnemonic information processing, and has been implicated in regulating the response of the hypothalamic-pituitary-adrenal (HPA) axis to stress(59).

Since $5HT_{1B}$ receptors inhibit synaptic transmission at CA1 to subicular synapses by modulation of the Gβγ-SNARE interaction(25), we compared the effects of application of the $5HT_{1B}$R selective agonist CP93129 on hippocampal slices prepared from age-matched WT or SNAP25Δ3 animals during field potential recordings in the subiculum after stimulation of CA1 pyramidal neuron axons. $GABA_A$R and NMDAR antagonists were applied to eliminate these currents and to focus on AMPAR-mediated EPSPs. The slope of excitatory postsynaptic potentials recorded in WT animals was inhibited in a concentration-dependent manner; specifically 400, 800, and 1600 nM of CP93129 caused a significant 50, 70, and 80% decrease in the EPSP slope, respectively (Fig. 4B left and bottom panels). By contrast, in hippocampal slices from the SNAP25Δ3 animals, 400, 800, and 1600 nM of CP93129 caused only 30, 35, and 40% decreases in the EPSP slope, respectively (Fig. 4B, right and bottom panels), a significant difference from EPSP suppression in WT mice. Overall, these data indicate that 5-HT_{1b}-mediated inhibition of exocytosis is decreased in the SNAP25Δ3 animals, suggesting that disruption of $5HT_{1b}$-mediated Gβγ-SNARE interaction in transgenic animals attenuates presynaptic inhibition.

No change in $GABA_B$–mediated inhibition of neurotransmission from the CA1 hippocampal region to the subiculum is detected in SNAP25Δ3 homozygotes

To examine if synaptic transmission, controlled by Gβγ inhibition of calcium through VGCCs, was altered in SNAP25Δ3 animals, we measured $GABA_B$-mediated inhibition of neurotransmission in the hippocampal CA1 to subicular synapse. The effect of the selective $GABA_B$ receptor agonist baclofen on field potential recordings did not differ between WT or SNAP25Δ3 animals (Fig. 4C). These data are consistent with the interpretation that Gβγ regulation of Ca^{2+} entry by baclofen is normal in the SNAP25Δ3 animals.

To determine whether the SNAP25Δ3 mutation impacted any cognitive functions in the mutant mice, we assessed potential differences between age-matched littermate WT and homozygotes in the Morris water maze task, a preclinical model of hippocampal-mediated spatial learning and memory(60,61) Homozygous SNAP25Δ3 mice required significantly longer than the WT mice to accurately identify the position of the hidden platform (Fig. 4D).

Gβγ regulation of Ca^{2+} entry and direct Gβγ inhibition of exocytosis at SNAREs provide synergistic inhibition of postsynaptic responses

Gβγ can mediate neuromodulatory effects through two different mechanisms, $GABA_B$-mediated inhibition of VGCC and Ca^{2+} entry and 5-HT_{1B}-mediated inhibition of exocytosis through Gβγ binding to the SNARE complex (25) (Fig. 5A). Consistently, Gβγ-SNARE inhibition is more pronounced at the first spike of a train and decreases with Ca^{2+} buildup, while inhibition through VDCCs is consistent throughout the train(62). Because we have shown that there is a temporal pattern to the effects of Gβγ on SNARE mediated exocytosis(62) we also examined trains of stimuli. When CA1 pyramidal neuron axons were stimulated repetitively to evoke EPSCs and subicular neurons were whole-cell clamped, the inhibition of the postsynaptic response by the 5-HT_{1b}R selective agonist CP93129 was not sustained but was attenuated by each consecutive stimulus (blue line, Fig 5B). The effect of CP93129 was diminished 4.6±0.8-fold by the fifth stimulus relative to the first, but the effect of baclofen was not significantly diminished by repetitive stimulation, with a ratio of 1.1±0.2 (Fig. 5c). This attenuation of the effect of CP93129 is interpreted to be due to Ca^{2+} buildup, allowing sytI to compete more effectively with Gβγ for binding to the SNARE complex(21,63).

By contrast, inhibition of Ca^{2+} entry by baclofen is not phasic in nature, generating a similar extent of inhibition of postsynaptic responses at each stimulus (green line, Fig 5B). To determine whether these distinct mechanisms of presynaptic inhibition were additive or more than additive, implying synergism, we examined the impact on inhibition of postsynaptic responses with a simultaneous administration of CP93129 and baclofen. The inhibitory response to this dual stimulation of 5-HT_{1b} and $GABA_B$ receptors was much greater than additive (red line, Fig 5C). We have previously shown that an unknown microarchitecture-forming component of the active zone determines whether presynaptic GPCRs signal through Gβγ-SNARE or Gβγ-VGCC (25) (Fig. 5A), but these mechanisms can also interact synergistically.

SNAP25Δ3 mice exhibit modest alterations in autonomic and somatomotor nervous system functions

To identify gross neurological deficits, we performed a modified Irwin Neurological Battery(64) on male homozygote SNAP25Δ3 and their age-matched littermate WT mice. This test battery evaluated changes in 25 different autonomic and/or somatomotor nervous system endpoints (Supplemental Figure 2, A and B). While the SNAP25Δ3 mice displayed no change in core body temperature, modest alterations in the aggregate Irwin scores for both the autonomic and somatomotor nervous system functions were noted relative to the WT mice reflecting differences in several endpoints, including the corneal and pinna reflexes, leg weakness, and placing loss, a parameter in which the animals is unable to immediately replace its hindlimb in its normal position when moved out of position (Supplemental Figure 2A, top and bottom panels). These deficits hinted towards the presence of potential impairments in $G_{i/o}$-coupled GPCR signaling and the need to follow-up with more extensive behavioral and physiological characterization of these mice, including assessment of specific autonomic nervous system functions, locomotor coordination, and nociception.

SNAP25Δ3 mice have impaired motor coordination

GPCRs, including those located presynaptically, mediate effects on locomotor behaviors throughout the neuraxis. These effects include supraspinal modulation of initiation of behaviors(65) and modification of output generated within the spinal cord(66) and involve various presynaptically expressed $G_{i/o}$-coupled receptors. To assess potential alterations in locomotor activity in the SNAP25Δ3 mouse, we evaluated overall locomotor activity using an open-field test. No significant genotype-based differences in the total distance traveled or rearing behaviors were observed at any interval over the entire 60 min test period in either light or dark conditions for WT and homozygote SNAP25Δ3 mice (Figure 6A and Supplemental Fig. S3, A and B).

We evaluated the motor coordination, balance, and learning of the SNAP25Δ3 mice using a multi-day rotarod paradigm in which the latency (in seconds) required for a mouse to drop from a constantly accelerating rotarod was measured over three consecutive days. Both the male WT and SNAP25Δ3 mice showed increased motor learning as denoted by increased latencies to drop from the rotarod on each subsequent day of testing (Fig. 6B). However, the rate of motor learning was decreased in the SNAP25Δ3 mice relative to the WT mice by the second day of testing.

SNAP25Δ3 mice do not differ from WT mice in anxiety in the absence of stressors, but have an increased rate of helplessness in the forced swim model

Similar to motor control, mood and affect are also modified by GPCRs. An important component of this effect is mediated by presynaptic $G_{i/o}$-coupled receptors including 5-HT_{1B} and α_{2A} adrenergic receptors, cannabinoid CB1 receptors, dopamine D1 and D2 receptors and group II mGluRs. We sought to investigate potential abnormalities in experimental models related to mood and affect in the SNAP25Δ3 homozygote mice. Using the light-dark box paradigm(67), a preclinical model of anxiogenic-like activity, we assessed whether SNAP25Δ3 mice would spend more or less time in the light portion of the testing chamber in comparison to the age-matched WT littermates. There were no significant differences between WT and homozygote SNAP25Δ3 mice in the time spent in the light side of the chamber, transitions between the light and dark sides of the chamber, or the distance traveled in the light and dark chambers (Supplementary Fig S4, A and B). These data suggest the absence of an anxiety-like phenotype in SNAP25Δ3 homozygotes in the absence of an external stressor.

We performed the forced swim test(68), a preclinical model for the evaluation of antidepressant efficacy. Age-matched WT and homozygotes were placed into an inescapable, water-filled cylinder and the latency to immobility and the total immobility times were recorded. SNAP25Δ3 homozygotes spent significantly more time immobile (Fig. 7A, left panel) than WTs and have a significantly lower latency to immobilization (Fig. 7A, right panel). These results are consistent with a potential depressive-like phenotype in the SNAP25Δ3 mice.

SNAP25Δ3 mice show altered supraspinal, but not spinal, nociception

Due to the potential for presynaptic modulatory effects of GPCRs in pain transmission, we follow-up by investigating whether the SNAP25Δ3 mutation altered either spinal or supraspinal mediated mechanisms of nociception, using the tail flick and hot plate assays, respectively(69). SNAP25Δ3 mice exhibited a decreased sensitivity to thermal pain in the hot plate paradigm in comparison to age-matched WT littermates (Fig. 7B, left panel) as shown by an increased latency to withdraw or lick the footpad after being placed on a 55°C hot plate. However, in the tail flick paradigm (a measure of spinal nociception), age-matched SNAP25Δ3 homozygotes and WT littermates did not show differences in tail withdrawal latency (Fig. 7B, right panel), indicating that SNAP25Δ3 homozygotes have alteration in supraspinal, but not spinal nociception, leading to increased pain thresholds.

DISCUSSION

We generated a transgenic mouse that contains a 3-amino acid truncation of SNAP25 at its C terminus, the SNAP25Δ3 mouse, based on our evidence that this mutant binds Gβγ less well than does the WT protein and that Gβγ-mediated modulation of exocytosis is impaired (26). This mouse model enabled us to investigate in vivo the effects of decreasing the neuromodulatory effects of $G_{i/o}$-coupled GPCRs that work by liberating Gβγ to bind to the SNARE complex and inhibit exocytosis directly. Though this modulatory mechanism has been described in vitro(14–17,21,26), here we describe *in vivo* phenotypes caused by its loss, including significant defects in nociception and stress handling, motor coordination, affective behaviors, and cognitive behaviors such as spatial learning.

Multiple independent groups have demonstrated that the SNAP25Δ3 mutant is not deleterious to exocytosis in neurons and chromaffin cells(26,45). Furthermore, Gβγ appears to be the only SNARE-binding protein that binds to the three C-terminal residues of SNAP25. This enabled us to selectively examine the effect of Gβγ−SNARE interactions *in vivo.* Gβγ directly competed with sytI for binding to t-SNARE made with SNAP25 WT, whereas it was less able to compete with sytI for binding to tSNARE made with SNAP25Δ3 (Fig. 2A). We confirmed that t-SNARE complexes consisting of SNAP25Δ3 did not show changes in synaptotagmin I-stimulated liposome fusion, with a maximal extent of lipid mixing not different from that of WT t-SNAREs. In addition, Gβγ-mediated inhibition of Ca^{2+}-sytI and SNARE-dependent lipid mixing was reduced with t-SNARE complexes consisting of SNAP25Δ3. Together, these data suggest that the specific phenotypes observed in SNAP25Δ3 homozygote neurons are due to a decreased ability of Gβγ to bind to SNARE complexes and displace sytI at the terminal.

Gβγ binding to the C-terminal region of SNAP25 was first identified by the effects of botulinum toxin type A (BoNT/A)-mediated cleavage of its C-terminal 9 residues on synaptic modulation(17). Gβγ liberated from $5HT_{1B}$ receptors inhibits exocytosis by displacing Ca^{2+}-dependent sytI binding to t-SNARE(16,21,27). This results in a phasic inhibition of synaptic transmission as calcium buildup during a train of action potentials enables sytI to compete more effectively with Gβγ for binding to the SNARE complex(21,63). As predicted, injection of EGTA eliminates the phasic inhibition during trains(21,63). Biochemically, competition between Gβγ and sytI depends upon the

concentrations of both Gβγ and sytI, demonstrating that this competition between Gβγ and Ca^{2+}-sytI interactions with the t-SNARE complex(21) is competitive. The ability of Gβγ to displace sytI is lost in SNAP25 mutants lacking identified Gβγ interaction sites, both in models of binding in aqueous solution and in models in which the SNARE complex is embedded in lipid bilayers(16,21,27). In this study, we confirmed that Gβγ competed less well with sytI for binding to t-SNARE consisting of SNAP25Δ3 than with t-SNARE consisting of WT SNAP25. As predicted, Gβγ-mediated inhibition of Ca^{2+}-sytI and SNARE-dependent lipid mixing was reduced with t-SNARE complexes containing SNAP25Δ3.

Conservation of the amino acid sequence in the C-terminus of SNAP25 is extremely high, particularly with regards to the C-terminal nine residues, which are conserved between mammals, birds, and reptiles, pointing to the evolutionary importance of this region. Vectorial assembly of the SNARE complex proceeds from the N- to the C-terminus(70), and the C-terminal region of the zippering SNARE complex is crucial for the generation of force leading to fusion pore formation. A truncation of the C-terminal 9 residues of SNAP25 leads to smaller foot currents and reduced fusion pore conductances(71,72), consistent with impaired vesicle-surface fusion events. Thus, it is interesting that Gβγ binding to the extreme C-terminus modifies fusion properties(73) and inhibits exocytosis, suggesting that it may interfere with fusion pore opening. Structural studies on the nature of the Gβγ-SNARE complex would elucidate the nature of this inhibitory mechanism. The high conservation of this region may also be required for tight control over exocytosis by regulation by $G_{i/o}$-coupled GPCRs of the Gβγ-SNARE interaction, which is present even in extremely primitive vertebrates, such as lamprey. Indeed, we have demonstrated this phenomenon in the primitive cartilaginous fish sea lamprey, which have giant axons in their spinal cord because of lack of myelination, enabling us to inject proteins presynaptically(15,17).

In SNAP25Δ3 animals, both the α_{2A}-ARs and the $5HT_{1b}R$, which function at least partially through Gβγ-SNARE(19,25,74), were unable to inhibit exocytosis to the same extent as they did in WT littermates. By contrast, in both the hippocampus and the bed nuclei of the stria terminalis (BNST) of SNAP25Δ3 animals, Gβγ inhibition did not affect exocytosis through the $GABA_B$ receptor, which functions through modulation of calcium entry. This showed that Gβγ responses through VGCCs, the major other membrane-delimited mechanism regulating neurotransmission, were not perturbed by the SNAP25Δ3 mutation. Furthermore, receptors working through both modulatory mechanisms can be present in the same synapse, as has been shown in electrophysiological studies in the hippocampus (25).

Although we do not know in most cases which mechanisms are activated by different GPCRs, and, indeed, these may be different in different neurons (29), we know that individual synapses can contain multiple $G_{i/o}$-coupled GPCRs. As previously reported (62), and as follows from direct Gβγ competition with sytI-SNARE interactions (Fig 2A), the effects of Gβγ-SNARE interaction are attenuated in response to trains of action potentials because of the buildup of residual Ca^{2+} during the course of a stimulus train (17). As Ca^{2+} concentrations in the presynaptic terminal rise, Ca^{2+}-sytI becomes a better competitor of Gβγ at the SNARE complex and Gβγ inhibition decreases (21). This opens the possibility that other signal transduction mechanisms within the presynaptic terminal can act

synergistically with the Gβγ−SNARE interaction. For example, at the CA1-subicular synapse, 5-HT_{1B} agonists cause Gβγ to interact directly with the SNARE complex. At the same synapse, $GABA_B$ receptors inhibit presynaptic Ca^{2+} entry, so that $GABA_B$ receptor activation reduces action potential-mediated increases in Ca^{2+} concentration during trains. When both receptors are activated, decreased residual Ca^{2+} buildup by $GABA_B$ receptor activation substantially enhances the 5-HT mediated inhibition during the stimulus train, leading to profound presynaptic inhibition. Such a dual modulation substantially increases the repertoire of presynaptic inhibition, potentially providing much greater control of transmission than either mechanism alone. The synergistic effect of simultaneous engagement of both neuromodulatory mechanisms at the same synapse raises the exciting possibility that therapeutic pairing of drugs that affect each mechanism may themselves work synergistically.

The two modulatory mechanisms have different characteristics. The inhibition of VDCCs by Gβγ is sensitive and powerful, but easy to saturate, whereas the Gβγ-SNARE interaction at the final step of membrane fusion is stoichiometric (meaning that there are one or two Gβγ proteins per SNARE) and phasic, based on Ca^{2+}-syt interactions, and thus may provide a much broader dynamic range of modulation that is more difficult to saturate. Gβγ interacts directly with the SNARE complex, providing a mechanism to modulate vesicle fusion, but without other known downstream effectors. The C-terminal region of SNAP25 is critical for forces associated with fusion pore formation, and stability (70,72,75). Indeed, consistent with this important role of the C-terminal region in fusion pore dynamics, the interaction of Gβγ with this target modifies fusion properties themselves as a mechanism of presynaptic inhibition(63,73,76). In constrast, receptors that simultaneously target presynaptic Ca^{2+} channels mediate a much broader range of presynaptic effects, from modifying action potential shape, to altering release probability, as well as modulating Gβγ effects at the SNARE complex by altering Ca^{2+} accumulation during stimulus trains.

As expected, stress responses in SNAP25Δ3 homozygotes were substantially enhanced, given that the major adrenergic autoreceptor that inhibits norepinephrine release works through this mechanism(77). We showed that the effect of the α_{2A}-AR selective agonist guanfacine on excitatory glutamatergic transmission in the dorsal BNST, a component of the extended amygdala, was nearly eliminated in brain slices from homozygous SNAP25Δ3 mice. The α_{2A}-AR presynaptically regulates excitatory input in the extended amygdala through a BoNT sensitive –mechanism regulated by Gβγ (19). Our results here provide further support for such a mechanism at these glutamatergic synapses. Heteroreceptor effects of α_{2A}-AR agonists, such as those shown, have marked outcomes on both physiologies within the extended amygdala(56–58) and on whole-organism behavior(77,78). Specifically, heteroreceptor α_{2A}-ARs are responsible for the sedation, anesthetic sparing, hypothermia, analgesia, bradycardia, and hypotension induced by systemic administration of α_{2A}-AR agonists(56). This contrasts with the autoreceptor α_{2A}-ARs, which are responsible for physiologic feedback inhibition of norepinephrine release and spontaneous locomotor activity(77). The relative contributions and deficits of auto- and hetero-receptor α_{2A}-ARs to the stress-related phenotypes observed in the SNAP25Δ3 mouse remain unclear and will be the focus of future studies investigating the mechanisms underlying the ability of α_{2A}-AR agonists to block the ability of stress to impact neurotransmission(79), depression- and

anxiety-related phenotypes(80,81) and drug-seeking behavior in rodent models of addiction(82–84).

The Gβγ-SNARE mechanism critically regulates vesicle release by $G_{i/o}$-coupled GPCRs in various secretory cell types, including multiple populations of neurons in the amgydala, cerebellum, spinal cord, and hippocampus(15,19,20,49), chromaffin cells(22), the beta cells of the islets of Langerhans(24), and cone photoreceptors(28). Here, we expand upon these existing findings. Presynaptic receptors have been thought to work mainly through modulation of Ca^{2+} entry by inhibiting VGCCs (2–10), or by activating GIRK channels(85,86). Using the SNAP25Δ3 mouse as a model of deficiency in the Gβγ-SNARE pathway, we demonstrated that selective inhibition of Gβγ-SNARE interaction results in multiple deleterious behavioral phenotypes associated with stress, locomotion, pain processing and spatial learning, as well as increased immobility in forced swim tests associated with depressive-like phenotype, implying downstream physiological and pathophysiological consequences for disruption of the Gβγ-SNARE pathway. We demonstrated a breadth of pathways and systems in which this mechanism is involved. In addition, this work permits us to draw general inferences on what is not dependent on the Gβγ-SNARE pathway: it is clear that neurotransmission is not completely unregulated in the absence of Gβγ-SNARE activity, leading to uncontrolled neuronal firing and seizure activity.

Neonatal lethality and gross deficits in exocytosis occur SNAP25-null homozygotes, but not in the SNAP25Δ3 homozygotes. Physiological consequences for disruption of SNAP25 function are also observed in the SNAP25b-deficient homozygotes, in which the exon specific to SNAP25b is replaced by a second SNAP25a exon(87), producing spontaneous seizures and behavioral deficits. SNAP25Δ3 homozygotes had locomotor deficiencies in the rotarod test that are similar in magnitude to the SNAP25 I67T homozygotes, a phenotype termed the “blind-drunk mouse”(88), although the SNAP25Δ3 homozygotes lack any of the deficits observed in the light-dark box test present in the I67T homozygotes. However, SNAP25Δ3 homozygotes did not show deficits in the elevated zero/plus maze paradigm or spontaneous seizure activity. A comparison of the phenotypes of the highly selective mutation in the SNAP25Δ3 mice compared to those of the SNAP25 null and SNAP25 I67T mice will help identify the particular molecular interactions, and the affinity/probability of these interactions, for more selective therapeutic target strategies, especially since the abundance of other presynaptic proteins, such as syntaxin 1a and Munc18, were not altered in SNAP25Δ3 homozygotes.

The substantial phenotypes displayed by SNAP25Δ3 homozygotes in many behavioral paradigms demonstrate that $G_{i/o}$-coupled GPCR regulation of Gβγ binding to the exocytotic fusion machinery is required for normal physiological and behavioral function. We are particularly interested in the GPCR identity and circuitry basis of the presynaptic inhibitory action of GPCRs underlying these changes. We currently do not know which $G_{i/o}$-coupled GPCRs work through this mechanism, but these mice will be useful to elucidate which GPCRs work through which mechanism. In addition, since the SNAP25Δ3 mutation is present in all cells in this mouse, further circuit-based studies will need to be carried out to understand the basis of the SNAP25Δ3 phenotypes. For example, viral expression of the

SNAP25–8A mutation that has no affinity for Gβγ(14) or use of tissue-specific channel rhodopsin to activate particular loci, will help to further define the circuitry underlying these behavioral phenotypes. Nevertheless, some circuit implications for these receptors can be made from experiments targeting specific receptor subtypes, with known and selective efficacy at the SNARE complex. These effects are consistent with defects found in the SNAP25Δ3 homozygous mice. In the lamprey spinal cord, 5-$HT_{1B/1D}$-like receptors are found on glutamatergic terminals of the descending motor command system and the locomotor pattern generator. Activation of these receptors in lamprey mimics the effects of 5-HT application in all vertebrate models of locomotion, in which locomotor frequency is lowered(63,89) Loss of these receptor-mediated effects in intact animals would be expected to lead to a loss of locomotor coordination and a reduction in the range of locomotor frequencies the animal can achieve. We observed evidence for this phenotype in the rotarod test in which the SNAP25Δ3 mice exhibited a decrease latency to drop from the rotatod.

Although many of the observed behaviors in the SNAP25Δ3 mutant mice remained unaltered, there were several clear phenotypic changes related to depressive-like activity and altered nociception. The SNAP25Δ3 mutant mice showed a decreased latency to immobilization with an overall increased time spent immobilized during the forced swim test consistent with a depressive-like phenotype. In addition, SNAP25Δ3 mutant mice exhibited an increased latency to withdrawal in the hot plate test suggesting possible disruptions in normal supraspinal-mediated nociceptive processes(69). While the exact mechanism(s) mediating these effects remains unclear, a possible explanation for these observed behavioral changes in the SNAP25Δ3 mutant mice is a decreased activation of presynaptic receptors that signal through the SNARE complex, such as 5-HT_{1B} and/or α_{2A} receptors, which inhibit transmitter release in WT mice; this effect on transmitter release would be decreased in SNAP25Δ3 mutant mice due to the compromised βγ−mediated signaling mechanism(101,104–107). Increased transmitter release at a circuit level could in turn explain the observed depressant-like phenotype and altered pain processing in SNAP25Δ3 mutant mice(102,103,108). Thus, our findings are consistent with the possibility that the Gβγ-SNARE manipulation has disrupted normal 5-HT and/or NE signaling related to depression-like and nociceptive behavior. In future studies we will examine the specific role of Gβγ in regulating circuitry related to mood and nocicpetive states and differentiate actions at pre- versus postsynaptically expressed receptors.

These studies provide a basis for the hypothesis that the Gβγ-SNARE interaction and modulation of exocytosis downstream of presynaptic Ca^{2+} entry is an important neuromodulatory mechanism in a large diversity of circuits, mediating multiple behaviors. The SNAP25Δ3 animal model will make the less-understood mechanism of Gβγ modulation of the SNARE complex easily studied on its own. Future studies will focus on identifying the $G_{i/o}$-coupled GPCRs that signal through Gβγ-SNARE and determining transcriptional signatures and pathologies related to this mechanism.

MATERIALS AND METHODS

Transgenic embryo generation

The SNAP25Δ3 mouse was generated with assistance from the Vanderbilt Transgenic Mouse and Embryonic Stem Cell Resource in compliance with protocols approved by the Vanderbilt Institutional Animal Care and Use Committee. Transgenic mouse embryos were generated utilizing the CRISPR/Cas9 system. The protospacer targeting construct was generated via a 24-mer oligo with a forward sequence of 5'CACCGCAACAAAGATGCTGGGAAG3' annealed to 5'AAACTTCCCAGCATCTTTGTTGC 3'. 1 μg of px330 vector (Zhang lab, MIT) was digested in a stoichiometric fashion with Bbs1 (NEB) to a final concentration of 50ng/μL for 1h at 37 C. The oligo was then ligated into the digested product with Quick Ligase (NEB) in a one-pot reaction in which oligo was added to a final concentration of 0.4 μM. and ligated for 4m at 25 C. Constructs were verified via Sanger sequencing. The single-stranded homology donor(IDT, Ultramer) was 126bp in length and spanned the C-terminal final exon of SNAP25 with 48bp of homology in either direction of the site of interest along with the G204* mutation and a HindIII site 3' of the G204* for the purposes of sequencing. The px330 vector and single-stranded homology donor were co-microinjected into the pronucleus of 587 B6D2 embryos, 447 of which were implanted into 40 B6D2 dams. 32 pups were obtained, two of which contained the G204* mutation in germline cells as measured by PCR analysis of genomic DNA. To verify that the inserted transcript was correct, PCR products were then excised and ligated into pCR2.1TOPO, which was then subjected to Sanger sequencing using M13 and T7 primers. No changes other than the addition of the G204* and HindIII site were observed.

Mouse breeding and genotyping

Littermate cohorts in this study carry a mixed genetic background of 75% C57BL/6J and 25% DBA2. The presence of the G204* mutation in the SNAP25Δ3 mouse was verified via PCR and Sanger sequencing. Genomic DNA was extracted from the fecal epithelium (Zymo Research) of weaned animals, and homozyogous SNAP25Δ3 animals were differentiated from WT littermates using two separate PCR reactions. Genomic DNA was amplified using a common reverse primer GGATTGTGGCAGTAGCTCG with diagnostic forward primers: the SNAP25Δ3-specific forward primer, 5' GATGCTGTAAGCTTAGTGG 3'; WT-specific forward primer, 5' GCAACAAAGATGCTGGGAAGTGG 3'. Amplicons generated are 467 bp and 459 bp respectively for SNAP25Δ3 and WT mice and were analyzed by agarose gel electrophoresis.

Plasmids

The open reading frames for syt I 96–421 was subcloned into the glutathione-s-transferase (GST) fusion vector, pGEX6p-1(90), (GE Healthcare, Chalfont St. Giles, Buckinghamshire, UK) for expression in *E.coli*. t-SNARE complexes consisting of SNAP25 and syntaxin1A were purified from the dual-expression vector pRSF-Duet1 with a subcloned N-terminal-His tag on SNAP25(91). C-terminally His-tagged synaptobrevin was produced from the plasmid pTW2[48]. The sequence corresponding to a gRNA specific to the final exon of SNAP25 was cloned into pX330-U6-Chimeric_BB-CBh-hSpCas9(92), which was a gift from Feng Zhang

(Addgene plasmid # 42230). t-SNAREs containing SNAP25Δ3 were produced by point mutagenesis of the WT SNAP25 sequence in pRSF-Duet1 using the method of overlapping primers. pCR2.1TOPO was obtained from Invitrogen.

Western blotting

For Western blotting analysis, antibodies against SNAP25 (Santa Cruz, sc-376713, 1:500), SNAP23 (Abcam, ab3340,1:500), cysteine string protein (Abcam, ab90499, 1:1000), tomosyn (Santa Cruz, Sc-136105, 1:1000), Hsc70 (Abcam, ab154415, 1:1000), Munc13-1 (Synaptic Systems, 126102, 1:1000), munc18-1 (Abcam, ab3451, 1:3000), synaptotagmin7 (Synaptic Systems, 105173, 1:1000), VAMP2 (Synaptic Systems, 104211, 1:1000), synaptotagmin1 (Synaptic Systems, 105-011, 1:1,000), complexin 1/2 (Synaptic Systems 122002, 1:500), syntaxin-1 (Santa Cruz, sc-12736, 1:2,000), and β-actin (Abcam, ab8227 1:5000) were used. HRP-conjugated secondary antibodies were obtained from Perkin-Elmer and used at the following dilutions: goat anti-mouse (1:10,000), and goat anti-rabbit (1:10,000). Images were analyzed for densitometry using ImageJ (available from http://rsbweb.nih.gov/ij/index.html). All statistical tests were performed using GraphPad Prism v.4.0 for Windows, (GraphPad Software, La Jolla, California, USA, www.graphpad.com).

Synaptosome preparation, fractionation, and lysate protocol

Crude synaptosomes were prepared, fractionated, and lysed from mouse brain tissue, as described previously(93). Various synaptic proteins were detected in lysate of whole crude synaptosomes and presynaptic fractions.

Protein purification and labeling

Recombinant bacterially expressed syntaxin1A and 6xHisSNAP25 (both WT and SNAP25Δ3 mutants) were expressed in tandem and purified from *E.coli* strain BL21. 6xHisVAMP2 was purified separately. GST-syt I 96–421 was purified separately on glutathione-agarose beads. All four proteins were purified according to previously published methods(27,47,48). $G\beta_1\gamma_1$ was purified from bovine retina as described previously(94). Purified syt I C2AB was buffer exchanged into 25 mM HEPES pH 7.4, 150 mM NaCl, 1 mM TCEP, and 10% glycerol and labeled at a 20-fold excess with Alexa Fluor 488-C5-maleimide at RT for 2H before excess probe was removed with an Amicon centrifugal filter with a molecular weight cutoff of 10,000.

Preparation of liposomes for fusion and TIRF assays

Small unilamellar liposomes containing t-SNARE complexes or VAMP2 were made as described previously(27,47,48). A volume of 55% POPC (1-Palmitoyl-2-Oleoyl-sn-glycero-3-phosphocholine), 15% DOPS (1,2-dioleoyl-*sn*-glycero-3-phospho-L-serine (sodium salt) and 30% POPE (1-Palmitoyl-2-Oleoyl-sn-glycero-3-phosphoethanolamine) in chloroform that would be equal to 15 mM of lipids in 100 μl were dried to a lipid film in a glass vial under argon, followed by vacuum removal of residual chloroform. Liposomes containing VAMP2 included 1.5% 1.5% N-(7-nitro-2-1,3-benzoxadiazol-4-yl)-1,2-dipalmitoyl phosphatidylethanolamine (NBD-PE) and 1.5% N-(lissamine rhodamine B sulfonyl)-1,2-dipalmitoyl phosphatidylethanolamine (Rhodamine-PE), along with 55%

POPC/15% DOPS/27% POPE. 0.4 mg of t-SNARE dimer or 95uL of VAMP2 was added to each tube of lipids in tandem with elution buffer 25 mM HEPES-KOH; pH 7.8, 400 mM KCl, 500 mM imidazole, 10% glycerol, 5 mM 2-mercaptoethanol, 1% n-octylglucoside) to a final volume of 500 μl and subjected to mild agitation until the lipid film was fully dissolved. Liposomes were then formed by adding 2 volumes of reconstitution buffer (25 mM HEPES-KOH, pH 7.8; 100 mM KCl; 1mM DTT; 10% glycerol;) in a dropwise manner, followed by additional mild agitation for 10 minutes. The solution was then dialyzed (10,000 molecular weight cutoff) twice for six hours in 4L of reconstitution buffer to remove residual detergent. Solutions were mixed with equivalent volumes of 80% iohexol (Accudenz, Accurate Chemical Co.) and were purified on a 0%/30%/40% iohexol gradient in a Beckman SW-55 swinging bucket rotor. Liposomes were harvested from the 0–30% interface and flash-frozen at - 80°C. Lipid concentrations and recovery rates were obtained using the Beer-Lambert law with NBD-PE absorbance at 460nm from v-SNARE liposomes containing NBD-PE that were maximally dequenched via the addition of docdeylmaltoside to 0.5%. SNARE protein concentrations in VAMP2 and t-SNARE liposomes were determined by Coomassie Brilliant Blue R-250 staining of SDS-PAGE gels containing a standard curve of bovine serum albumin (Thermo Scientific) followed by densitometric analysis of pixel intensity of syntaxin1A bands utilizing the Fiji distribution of ImageJ software(95,96). SNARE copy number in liposomes was determined according to previously published methods(47).

In membrane TIRF imaging

Lipid bilayers were prepared from liposomes containing 55% phosphatidylcholine, 15% phosphatidylethanolamine, and 29% phosphatidylserinein addition to 1% DiD (3,3′-Dioctadecyloxacarbocyanine perchlorate) with or without t-SNARE complexes containing WT or mutant SNAP25. TIRF imaging studies were conducted according to previously published methods(27). A shallow volume (to ~150 nm above the cover slip) was illuminated using TIRF on a custom microscope utilizing a laser launch with 488 nm solid state and 633 nm HeNe lasers whose output intensities were controlled using a Acoutic-Optical-Transmission Filter (AOTF, Prairie Technologies). 488 nm laser intensities at the microscope input used to illuminate fluorescently tagged proteins were 2 to 5 mW. This beam was offset and focused on the objective backplane (Olympus PlanApoN 60× 1.45 TIRFM) using a modified TIRF laser launch (Olympus IX2). Coverslips were 0.17 mm borosilicate glass. After laying down lipids in a 5 mM $CaCl_2$-containing solution to induce fusion of WT or mutant t-SNARE complexes with the lipids, a superfusate consisting of 150 mM KCl and 5 mM HEPES was applied at a rate of 1mL/min for 30 min. Then AF-sytI with 100 μM free Ca^{2+} was applied in solution over the cover-slip-supported lipid bilayer. Increasing concentrations of Gβγ were then applied in this 100 μM Ca^{2+} solution and AF-sytI fluorescence was then measured. The 633 nm excitation was used to focus the TIRF illumination on the bilayer. Simultaneously, the intensity and polarization of 535nm fluorescence emitted from Alexa Fluor 488-labeled syt1 C2AB (AF-syt1) was measured by capturing P and S polarized emission across a polarizing cube beamsplitter(27). The focus and setting of the TIRF field used a camera in the inverted configuration light path. Emission was detected and quantified through a second water immersion lens to minimize loss of

polarity in emission, with excitation light polarity in plane with one detector and orthogonal to another after a polarizing beam splitter.

Mice

All studies were conducted in adult male wildtype and SNAP25Δ3 homozygote mice that were bred in house as described above and group-housed unless specified under a 12/12 h light-dark cycle with water available *ad libitum*. All behavioral studies were evaluated in cohorts of age-matched, littermate controlled wildtype and SNAP25Δ3 homozygote mice. All animal experiments were approved by the Vanderbilt University Animal Care and Use Committee and experimental procedures conformed to guidelines established by the National Research Council Guide for the Care and Use of Laboratory Animals. All efforts were made to minimize animal suffering and the number of animals used.

Modified Irwin Neurological Test Battery and Body Weights

This test battery evaluated changes in 25 different autonomic and/or somatomotor nervous system endpoints using the Modified Irwin Neurological Test Battery(64) in age-matched littermate male SNAP25Δ3 homozygotes (n= 21) or wild-type (n= 17) of 14–15 weeks of age. All data were manually collected by an experimenter blinded to genotype. Data were represented as the aggregate mean scores for the autonomic or somatomotor nervous system endpoints of the Irwin test battery per genotype and were analyzed by Student's t-test using GraphPad Prism. Differences were evaluated using a rating scale from 0–2 with 0 indicating no effect, 1 indicating modest effects, and 2 indicating robust effect. The aggregate mean scores were extrapolated by calculating the sum of each Irwin parameter for all mice tested. Then the mean of the autonomic or somatomotor parameters were calculated. Data are represented as means ± SEM and were analyzed by Student's two-tailed t-test using GraphPad Prism. In addition, total body weight in grams (g) was measured between 3–60 weeks of age for WT and SNAP25Δ3 homozygote mice. Data are presented as means ± SEM and were analyzed by two-way ANOVA using GraphPad Prism.

Stress induced hyperthermia assay

Singly-housed male SNAP25Δ3 homozygotes or wild-type littermate controls were allowed to acclimate to the testing room for 60 minutes. Baseline temperature was taken by inserting a BAT-12 Microprobe Thermometer, dipped into mineral oil, 2 cm into the rectum for each mouse for 20 s to obtain core body temperature (T_1). After a 15-min interval, core body temperature for each mouse was measured a second time (T_2). Stress-induced hyperthermia was calculated as the change in core body temperature between the first and second temperature readings ($\Delta T = T_2 - T_1$) based on previously published methods(54) Data are presented as means ± SEM and were analyzed by Student's two-tailed t-test using GraphPad Prism.

Locomotor Activity Assay

Open field activity was tested in age-matched 10–12 week old male WT (n=15) and homozygote SNAP25Δ3 animals (n=14) using an open field system (OFA-510, MedAssociates, St. Albans, VT) with three 16 × 16 arrays of infrared photobeams as

previously described(97). Total number of photobeam breaks were collected over 60 min under light or infrared lighting conditions. Data were calculated as either the mean distance traveled (cm) ± SE for the number of photobeam breaks/5 min bin/genotype, the total distance traveled (mean horizontal and vertical beam breaks/30 mins) or the total rearing behavior (mean vertical beam breaks/30 mins. Data are presented as means ± SEM and were analyzed by two-way ANOVA (mean distance traveled) and Student's two-tailed t-test (total distance traveled and rearing) using GraphPad Prism.

Tail-Flick Test

Age-matched littermate male SNAP25Δ3 homozygotes or WT controls were assessed in the tail-flick assay, a preclinical model of acute spinal-mediated thermal nociception(69). All mice had their tails individually immersed in a water bath maintained at 55°C, and the latency to removal in sec was measured. If an animal did not flick its tail within 10 s, it was removed and assigned a response time of 10 s. Data are presented as means ± SEM and were analyzed by Student's two-tailed t-test using GraphPad Prism.

Hot Plate Test

Age-matched littermate male SNAP25Δ3 homozygotes or WT controls were assessed in the hot plate assay, a preclinical model of acute supraspinal-mediated thermal nociception(69).All mice were individually placed on a hot plate maintained at 50–55°C and the latency to lick the front or hind paws was recorded for each mouse. Animals not responding within 30 s were removed and assigned a score of 30 s. Data are presented as means ± SEM and were analyzed by Student's two-tailed t-test using GraphPad Prism.

Rotarod assay

Age-matched 10–12 week old male WT (n=15) and homozygote SNAP25Δ3 animals (n=14) were assessed for their ability to maintain balance upon a rotating cylinder undergoing constant acceleration from 4 to 40 RPM(98). The cylinder was 3cm in diameter and each animal was confined to approximately 6cm of cylinder length with Plexiglas dividers. Cylinders were suspended 25cm above a lever that actuates the timer, resulting in a stoppage of the timer to permit tabulation of the latency required for the animal to fall off the cylinder. The maximum length for each trial was 300 sec, at which point a maximum latency value of 300 was tabulated. Trials were conducted for three consecutive days. Data for each day were represented as the mean latency to drop from the rotarod in sec ± SE and analyzed using Student's two-tailed t-test for comparisons by day using GraphPad Prism.

Light-dark exploration

Anxiety responses were assessed in age-matched WT or SNAP25Δ3 homozygote male mice in a plastic cubic light-dark chamber 20 cm in length(67). A black opaque Plexiglas insert was utilized to selectively create darkness in half of the chamber. Animals were placed individually in each chamber for 5 minutes, and animal movement was recorded by the breaking of photobeams emitted by infrared photocells in each chamber. Time spent in the light side of the chamber (sec), number of transitions made by each mouse between the light and dark sides of the chamber, and distance traveled in the light and the dark sides of the

testing chamber (cm) were recorded. Data are represented as means ± SEM and were analyzed by Student's two-tailed t-test using GraphPad Prism.

Forced Swim Task

Age-matched littermates 16–17-week old WT (n= 14) or SNAP25Δ3(n=17) homozygote male mice were tested in forced swim paradigm(68). The depth of the water was such that the mice tail does not touch the bottom, but also prevents them from escaping the apparatus. For testing, each mouse was placed in the cylinder for 6 mins, and the latency to immobility and the immobility time (the time during which mice made only the small movements necessary to keep their heads above water) was scored. Only the data scored during the last 4 min were analyzed. Data are represented as means ± SEM and were analyzed by Student's two-tailed t-test using GraphPad Prism.

Morris Water Maze

Mice were trained to locate a hidden platform in a standard fixed platform memory acquisition task, in which the platform remained in a constant position (61). This acquisition phase lasted for six sessions, each of which consisted of four trials separated by approximately 10 min. Four points along the perimeter of the maze, served as starting points where the mice were released, facing the wall of the tank, at the beginning of each trial (the order of the starting points were determined randomly, except that each starting point was used only once each session). After a mouse located the platform, it was allowed to remain there for 30 s before being removed from the tank. If a mouse failed to locate the platform within 60 s, it was manually guided to it and again allowed to remain on the platform for 30 s. Data are represented as means ± SEM and were analyzed by Two-way ANOVA using GraphPad Prism.

BNST Electrophysiological analyses

Adult mice (>8 weeks) were single housed in the institutional vivarium prior to experiments. Food and water were available ad libitum. All procedures were approved by the Animal Care and Use Committee at Vanderbilt University. Mice were transported from the animal colony to the laboratory and allowed to acclimate in a sound-attenuation chamber for >1 hour before the experiment. They were then anesthetized with isoflurane until unresponsive to foot pinch. The mice were transcardially perfused with ice-cold sucrose-substituted artificial cerebrospinal fluid (ACSF) (in mM: 194 sucrose, 20 NaCl, 4.4 KCl, 2 $CaCl_2$, 1 $MgCl_2$, 1.2 NaH_2PO_4, 10.0 glucose, and 26.0 $NaHCO_3$) saturated with 95% O_2/5% CO_2. They were then decapitated and the brain was quickly removed and placed in ice-cold sucrose ACSF. Slices 300 μm thick containing the bed nucleus of the stria terminalis (bregma +0.26 to +0.14 mm) were prepared using a Tissue Slicer (Leica). After dissection, slices were transferred to a holding chamber containing heated (~29°C) oxygenated (95% O_2/5% CO_2) ACSF (in mM: 124 NaCl, 4.4 KCl, 2 $CaCl_2$, 1.2 $MgSO_4$, 1 NaH_2PO_4, 10.0 glucose, 26.0 $NaHCO_3$; pH 7.2–7.4; 295–305 mOsm). Recording electrodes (0.5–2 MΩ) were pulled on a Flaming-Brown Micropipette Puller (Sutter Instruments) using thin-walled borosilicate glass capillaries. Excitatory field potentials were evoked by local fiber stimulation with bipolar nichrome electrodes. Electrical stimulation (1–15 V with 5 ms duration) was applied at 0.0167 Hz. Recording electrodes were filled with ACSF and all experiments were done in

the presence of 25 μM picrotoxin to isolate fast excitatory transmission. Signals were acquired via a Multiclamp 700B amplifier (Axon Instruments), and digitized and analyzed via pClamp 10.2 software (Axon Instruments). The fiber volley potential (N1) was monitored continuously throughout the duration of the experiment. Experiments in which N1 changed by 20% in either direction were not included in subsequent analysis. Experiments were analyzed by measuring peak amplitudes of the N1 and N2 (synaptic potential) relative to the amplitude with no stimulation. This measure was then normalized to the last ten minutes of the baseline period (10–20 minutes). Welch's t-test was used to compare the average amplitude over the last 20 minutes of the experiment relative to baseline across the two genotypes.

Subiculum Electrophysiological Analyses

All procedures were approved by the Animal Care and Use Committee at Vanderbilt University and at the University of Illinois at Chicago. Male and female adult mice (>8 weeks) were obtained from the institutional vivarium prior to experiments, where food and water were available ad libitum. Mice were transported from the animal colony to the laboratory and allowed to acclimate for >1 hour before the experiment. They were then anesthetized with isoflurane until unresponsive to foot pinch. The mice were decapitated and the brain was quickly removed and placed in ice-cold sucrose-substituted ACSF (in M: 11 D-Glucose, 234 sucrose, 2.5 KCl, 1.25 NaH_2PO_4, 10 $MgSO_4$, and 26 $NaHCO_3$; in mM: 0.5 $CaCl_2$,) saturated with 95% O_2/5% CO_2. Slices 300 μm thick containing the hippocampus and subiculum were prepared using a Tissue Slicer (Leica VT1200S). After dissection, slices were transferred to a holding chamber containing oxygenated (95% O_2/5% CO_2) ACSF (in mM: 123 NaCl, 26 $NaHCO_3$, 3 KCl, 1.25 NaH_2PO_4, 11 D-Glucose; 2 $CaCl_2$, 1 $MgCl_2$; pH 7.2–7.4; 295–305 mOsm) for 45 minutes in a heated (~30°C) water bath then moved to room temperature for storage. Recording electrodes (3–5 MΩ filled with ACSF) were pulled on a Flaming-Brown Micropipette Puller (Sutter Instruments) using standard-walled borosilicate glass capillaries. Excitatory field potentials were evoked by local fiber stimulation with bipolar twisted insulated NiChrome electrodes in an interface chamber (Warner, BSC-BUW) heated to ~30°C. Electrical stimulation (200μs at 30 to 60 μA range) was applied every 30 seconds. All experiments were done in the presence of 10 μM bicuculline to black $GABA_A$ receptors and 50 μM D-2 amino-5-phosphonopentanoate (D-AP5) to block NMDA receptors to isolate AMPAR-mediated EPSPs. Signals were acquired via an Axoclamp 2B amplifier (Axon Instruments) amplified 100 x and band pass filtered (0.1 to 5KHz), and digitized and analyzed via AxographX version 1.6.5 software. Experiments were analyzed by measuring the initial slope of the excitatory postsynaptic potential and then normalized to the last ten minutes of the baseline period (20 minutes). Student's t-test was used to compare the average slope over the last 10 minutes of each dose of CP93129 (0, 50, 100, 200, 400, 800, and 100 nM) or baclofen (0, 0.5, 1, 2, 5, and 10 μM) concentrations relative to baseline across the wild-type and SNAP25Δ3 genotypes.

Statistical analysis: Statistical analyses were performed as denoted in the figure legends and tabulated with GraphPad Prism v.4.0. (GraphPad Software). n values in the text refer to the number of biological replicates contained within a study.

Supplementary Material

Refer to Web version on PubMed Central for supplementary material.

Acknowledgments:

We thank Jennifer Skelton and the Vanderbilt Transgenic Mouse and Embryonic Stem Cell Resource (supported by NIH grants CCSG CA68485 and DRTC DK020593) for assistance in the creation of the SNAP25Δ3 mouse. We thank the Vanderbilt High-throughput Screening Core for providing instrumentation for lipid mixing experiments. We thank John Allison, Ph.D and the Vanderbilt Murine Neurobehavioral Core for providing training and instrumentation for the behavioral studies conducted upon the SNAP25Δ3 mouse. We thank Bob Matthews Ph.D and the Vanderbilt Cell Imaging Shared Resource (supported by NIH grants CA68485, DK20593, DK58404, DK59637, and Ey08126) for training and instrumentation in microscopy. We thank Mark Fulton and Kayla Jo Temple for assistance in liposome production, and the laboratory of Feng Zhang, Ph.D (Massachusetts Institute of Technology) and Addgene for the gift of the px330 plasmid.

Funding: The work in this paper was supported by R01EY010291; R01MH101679 and R01DK109394 to HEH; R01MH 08487 to STA; R01DA042475 and F30DA042501 to DGW.

REFERENCES AND NOTES

1. Leenders AGM & Sheng Z-H Modulation of neurotransmitter release by the second messenger-activated protein kinases: Implications for presynaptic plasticity. Pharmacology & therapeutics 105, 69–84 (2005). [PubMed: 15626456]
2. Dunlap KF, GD. Neurotransmitters decrease the calcium component of sensory neurone action potentials. Nature 276, 837–839 (1978). [PubMed: 31570]
3. Bean BP Neurotransmitter inhibition of neuronal calcium currents by changes in channel voltage dependence. Nature 340, 153–156 (1989). [PubMed: 2567963]
4. Miller RJ Presynaptic receptors. Annual Reviews in Pharmacology and Toxicology 38, 201–227 (1998).
5. Herlitze S, Garcia DE, Mackie K, Hille B, Scheuer T, and Catterall WA Modulation of Ca2+ channels by G-protein bg subunits. Nature 380, 258–262 (1996). [PubMed: 8637576]
6. Ikeda SR Voltage-dependent modulation of N-type calcium channels by G-protein beta gamma subunits. Nature 380, 255–258 (1996). [PubMed: 8637575]
7. De Waard M, Liu H, Walker D, Scott VE, Gurnett CA & Campbell KP Direct binding of G-protein betagamma complex to voltage-dependent calcium channels [see comments]. Nature 385, 446–450 (1997). [PubMed: 9009193]
8. Zhang JF, Ellinor PT, Aldrich RW & Tsien RW Multiple structural elements in voltage-dependent Ca^{2+} channels support their inhibition by G proteins. Neuron 17, 991–1003 (1996). [PubMed: 8938130]
9. Zamponi GW, Bourinet E, Nelson D, Nargeot J. & Snutch TP Crosstalk between G proteins and protein kinase C mediated by the calcium channel alpha1 subunit. Nature. 385, 442–446. (1997). [PubMed: 9009192]
10. Dolphin AC Mechanisms of modulation of voltage-dependent calcium channels by G proteins. J Physiol 506 (Pt 1), 3–11 (1998). [PubMed: 9481669]
11. Logothetis DE, Kurachi Y, Galper J, Neer EJ & Clapham DE The betagamma subunits of GTP-binding proteins activate the muscarinic K+ channel in heart. Nature 325, 321–326 (1987). [PubMed: 2433589]
12. Reuveny E, Slesinger PA, Inglese J, Morales JM, Iniguez-Lluhi JA, Lefkowitz RJ, Bourne HR, Jan YN & Jan LY Activation of the cloned muscarinic potassium channel by G protein βγ subunits. Nature 370, 143–146 (1994). [PubMed: 8022483]
13. Wickman KD, Iniguez-Lluhi JA, Davenport PA, Taussig R, Krapivinsky GB, Linder ME, Gilman AG & Clapham DE Recombinant G-protein βγ subunits activate the muscarinic-gated atrial potassium channel. Nature 368, 255–257 (1994). [PubMed: 8145826]

14. Wells CA, Zurawski Z, Betke KM, Yim YY, Hyde K, Rodriguez S, Alford S. & Hamm HE Gβγ Inhibits Exocytosis via Interaction with Critical Residues on Soluble N-Ethylmaleimide-Sensitive Factor Attachment Protein-25. Molecular Pharmacology 82, 1136–1149 (2012). [PubMed: 22962332]
15. Blackmer T, Larsen EC, Takahashi M, Martin TF, Alford S. & Hamm HE G protein betagamma subunit-mediated presynaptic inhibition: regulation of exocytotic fusion downstream of Ca^{2+} entry. Science 292, 293–297. (2001). [PubMed: 11303105]
16. Blackmer T, Larsen EC, Bartleson C, Kowalchyk JA, Yoon EJ, Preininger AM, Alford S, Hamm HE & Martin TF G protein betagamma directly regulates SNARE protein fusion machinery for secretory granule exocytosis. Nat Neurosci 8, 421–425 (2005). [PubMed: 15778713]
17. Gerachshenko T, Blackmer T, Yoon EJ, Bartleson C, Hamm HE & Alford S. Gbetagamma acts at the C terminus of SNAP-25 to mediate presynaptic inhibition. Nat Neurosci 8, 597–605 (2005). [PubMed: 15834421]
18. Chen XK, Wang LC, Zhou Y, Cai Q, Prakriya M, Duan KL, Sheng ZH, Lingle C. & Zhou Z. Activation of GPCRs modulates quantal size in chromaffin cells through Gβγ and PKC. Nat Neurosci 8, 1160–1168 (2005). [PubMed: 16116443]
19. Delaney AJ, Crane JW & Sah P. Noradrenaline Modulates Transmission at a Central Synapse by a Presynaptic Mechanism. Neuron 56, 880–892, (2007). [PubMed: 18054863]
20. Glitsch M. Selective Inhibition of Spontaneous But Not Ca2+-Dependent Release Machinery by Presynaptic Group II mGluRs in Rat Cerebellar Slices. Journal of Neurophysiology 96, 86 (2006). [PubMed: 16611839]
21. Yoon EJ, Gerachshenko T, Spiegelberg BD, Alford S, and Hamm HE Gβγ interferes with Ca2+-dependent binding of synaptotagmin to the soluble N-ethylmaleimide-sensitive factor attachment protein receptor (SNARE) complex. Mol. Pharmacol. 72, 1210–1219 (2007). [PubMed: 17715396]
22. Yoon EJ, Hamm HE, and Currie KPM G protein βγ subunits modulate the number and nature of exocytotic fusion events in adrenal chromaffin cells independent of calcium entry. J Neurophysiol 100, 2929–2939. (2008). [PubMed: 18815342]
23. Iremonger KJ & Bains JS Retrograde Opioid Signaling Regulates Glutamatergic Transmission in the Hypothalamus. The Journal of Neuroscience 29, 7349 (2009). [PubMed: 19494156]
24. Zhao Y, Fang Q, Straub SG, Lindau M. & Sharp GWG Noradrenaline inhibits exocytosis via the G protein bg subunit and refilling of the readily releasable granule pool via the $a_i1/2$ subunit. The Journal of Physiology 588, 3485–3498 (2010). [PubMed: 20643776]
25. Hamid E, Church E, Wells CA, Zurawski Z, Hamm HE & Alford S. Modulation of Neurotransmission by GPCRs Is Dependent upon the Microarchitecture of the Primed Vesicle Complex. The Journal of Neuroscience 34, 260–274, (2014). [PubMed: 24381287]
26. Zurawski Z, Rodriguez S, Hyde K, Alford S. & Hamm HE Gβγ Binds to the Extreme C Terminus of SNAP25 to Mediate the Action of Gi/o-Coupled G Protein–Coupled Receptors. Molecular Pharmacology 89, 75–83 (2016). [PubMed: 26519224]
27. Zurawski Z, Page B, Chicka MC, Brindley RL, Wells CA, Preininger AM, Hyde K, Gilbert JA, Cruz-Rodriguez O, Currie KPM, Chapman ER, Alford S. & Hamm HE Gβγ directly modulates vesicle fusion by competing with synaptotagmin for binding to neuronal SNARE proteins embedded in membranes. Journal of Biological Chemistry 292(29):12165–12177 (2017).
28. Van Hook MJ, Babai N, Zurawski Z, Young Yim Y, Hamm HE & Thoreson WB A presynaptic group III mGluR recruits Gβγ/SNARE interactions to inhibit synaptic transmission by cone photoreceptors in the vertebrate retina. The Journal of Neuroscience, (2017).
29. Betke KM WC, Hamm HE. GPCR mediated regulation of synaptic transmission. Prog Neurobiol. 3 (2012).
30. Dolphin AC & Scott RH Calcium channel currents and their inhibition by (−)-baclofen in rat sensory neurones: modulation by guanine nucleotides. Journal of Physiology, London 386, 1–17 (1987).
31. Wu LG & Saggau P. Adenosine inhibits evoked synaptic transmission primarily by reducing presynaptic calcium influx in area CA1 of hippocampus. Neuron 12, 1139–1148 (1994). [PubMed: 8185949]

32. Tedford HW & Zamponi GW Direct G Protein Modulation of Cav2 Calcium Channels. Pharmacological Reviews 58, 837 (2006). [PubMed: 17132857]
33. Proft J. & Weiss N. G Protein Regulation of Neuronal Calcium Channels: Back to the Future. Molecular Pharmacology 87, 890 (2015). [PubMed: 25549669]
34. Augustine GJ & Charlton MP Calcium dependence of presynaptic calcium current and post-synaptic response at the squid giant synapse. The Journal of Physiology 381, 619–640 (1986). [PubMed: 2442355]
35. Dodge FA Jr. & Rahamimoff R. Co-operative action a calcium ions in transmitter release at the neuromuscular junction. J Physiol 193, 419–432 (1967). [PubMed: 6065887]
36. Mizutani H, Hori T. & Takahashi T. 5-HT1B receptor-mediated presynaptic inhibition at the calyx of Held of immature rats. European Journal of Neuroscience 24, 1946–1954, (2006).
37. Takahashi T, Forsythe ID, Tsujimoto T, Barnes-Davies M. & Onodera K. Presynaptic Calcium Current Modulation by a Metabotropic Glutamate Receptor. Science 274, 594 (1996). [PubMed: 8849448]
38. Scanziani M, Capogna M, Gähwiler BH & Thompson SM Presynaptic inhibition of miniature excitatory synaptic currents by baclofen and adenosine in the hippocampus. Neuron 9, 919–927, (1992). [PubMed: 1358131]
39. Scanziani M, Gahwiler BH & Thompsom SM Presynaptic inhibition of excitatory synaptic transmission by muscarinic and metabotropic glutamate receptor activation in the hippcampus: are Ca2+ channels involved? Neuropharmacology 34, 1549–1557 (1995). [PubMed: 8606802]
40. Silinsky EM On the mechanism by which adenosine recptor activation inhibits the release of acetylcholine from motor nerve endings. Journal of Physiology 346, 243–256 (1984).
41. Silinsky EM & Solsona CS Calcium currents at motor nerve endings: absence of effects of adenosine receptors agonists in the frog. Journal of Physiology, London 457, 315–328 (1992).
42. Luini A. & De Matteis MA Evidence that the receptor-linked G protein inhibits exocytosis by a post-second messenger mechanism in AtT-20 cells. Journal of Neurochemistry 54, 30–38 (1990). [PubMed: 1967144]
43. Scholz KP & Miller RJ Inhibition of quantal transmitter release in the absence of calcium influx by a G protein linked adenosine receptor at hippocampal synapses. Neuron 8, 1139–1150 (1992). [PubMed: 1351733]
44. Dittman JS & Regehr WG Contributions of calcium-dependent and calcium-independent mechanisms to presynaptic inhibition at a cerebellar synapse. The Journal of Neuroscience 16, 1623 (1996). [PubMed: 8774431]
45. Criado M, Gil A, Viniegra S. & Gutiérrez LM A single amino acid near the C terminus of the synaptosomeassociated protein of 25 kDa (SNAP-25) is essential for exocytosis in chromaffin cells. Proceedings of the National Academy of Sciences 96, 7256–7261, (1999).
46. Bouyer K. & Simerly RB Neonatal Leptin Exposure Specifies Innervation of Presympathetic Hypothalamic Neurons and Improves the Metabolic Status of Leptin Deficient Mice. The Journal of Neuroscience 33, 840–851, (2013). [PubMed: 23303959]
47. Tucker WC, Weber T. & Chapman ER Reconstitution of Ca^{2+}-regulated membrane fusion by synaptotagmin and SNAREs. Science 304, 435–438 (2004). [PubMed: 15044754]
48. Weber T, Zemelman BV, McNew JA, Westermann B, Gmachl M, Parlati F, Sollner TH & Rothman JE SNAREpins: minimal machinery for membrane fusion. Cell 92, 759–772 (1998). [PubMed: 9529252]
49. Zhang X. l., Upreti C. & Stanton PK Gβγ and the C Terminus of SNAP-25 Are Necessary for Long-Term Depression of Transmitter Release. PLoS ONE 6, e20500.
50. Starke K. Influence of extracellular noradrenaline on the stimulation-evoked secretion of noradrenaline from sympathetic nerves: Evidence for an α-receptor-mediated feed-back inhibition of noradrenaline release. Naunyn-Schmiedeberg's Archives of Pharmacology 275, 11–23, (1972).
51. Hein L. Adrenoceptors and signal transduction in neurons. Cell and Tissue Research 326, 541–551 (2006). [PubMed: 16896948]
52. Altman JD, Trendelenburg AU, MacMillan L, Bernstein D, Limbird L, Starke K, Kobilka BK & Hein L. Abnormal Regulation of the Sympathetic Nervous System in α_{2a}-Adrenergic Receptor Knockout Mice. Molecular Pharmacology 56, 154–161, (1999). [PubMed: 10385696]

53. Hein L, Altman JD & Kobilka BK Two functionally distinct α_2-adrenergic receptors regulate sympathetic neurotransmission. Nature 402, 181, (1999). [PubMed: 10647009]
54. Bouwknecht JA, Hijzen TH, van der Gugten J, Maes RAA & Olivier B. Stress-induced hyperthermia in mice: effects of flesinoxan on heart rate and body temperature. European Journal of Pharmacology 400, 59–66, (2000). [PubMed: 10913585]
55. Enero MA, Langer SZ, Rothlin RP & Stefano FJE Role of the α-adrenoceptor in regulating noradrenaline overflow by nerve stimulation. British Journal of Pharmacology 44, 672–688 (1972). [PubMed: 4339385]
56. Egli RE, Kash TL, Choo K, Savchenko V, Matthews RT, Blakely RD & Winder DG Norepinephrine Modulates Glutamatergic Transmission in the Bed Nucleus of the Stria Terminalis. Neuropsychopharmacology 30, 657–668 (2004).
57. Shields AD, Wang Q. & Winder DG α2A-adrenergic receptors heterosynaptically regulate glutamatergic transmission in the bed nucleus of the stria terminalis. Neuroscience 163, 339–351, (2009). [PubMed: 19527774]
58. Flavin SA, Matthews RT, Wang Q, Muly EC & Winder DG α_{2A}-Adrenergic Receptors Filter Parabrachial Inputs to the Bed Nucleus of the Stria Terminalis. The Journal of Neuroscience 34, 9319–9331, (2014). [PubMed: 25009265]
59. O'Mara S. The subiculum: what it does, what it might do, and what neuroanatomy has yet to tell us. Journal of Anatomy 207, 271–282, (2005). [PubMed: 16185252]
60. McNamara RK & Skelton RW Baclofen, a selective GABAB receptor agonist, dose-dependently impairs spatial learning in rats. Pharmacology Biochemistry and Behavior 53, 303–308, (1996).
61. Morris R. Developments of a water-maze procedure for studying spatial learning in the rat. Journal of Neuroscience Methods 11, 47–60, (1984). [PubMed: 6471907]
62. Takahashi M, Freed R, Blackmer T. & Alford S. Calcium influx-independent depression of transmitter release by 5-HT at lamprey spinal cord synapses. J Physiol 532, 323–336 (2001). [PubMed: 11306653]
63. Gerachshenko T, Schwartz E, Bleckert A, Photowala H, Seymour A. & Alford S. Presynaptic G protein-coupled receptors dynamically modify vesicle fusion, synaptic cleft glutamate concentrations and motor behavior. The Journal of Neuroscience 29, 10221–10233, (2009). [PubMed: 19692597]
64. Irwin S. Comprehensive observational assessment: Ia. A systematic, quantitative procedure for assessing the behavioral and physiologic state of the mouse. Psychopharmacologia 13, 222–257, (1968). [PubMed: 5679627]
65. Ford CP The role of D2-autoreceptors in regulating dopamine neuron activity and transmission. Neuroscience 282, 13–22, (2014). [PubMed: 24463000]
66. Alford S, Schwartz E. & Prisco GVD The Pharmacology of Vertebrate Spinal Central Pattern Generators. The Neuroscientist 9, 217–228, (2003). [PubMed: 15065817]
67. Takao K. & Miyakawa T. Light/dark Transition Test for Mice. Journal of Visualized Experiments : JoVE, 104, (2006).
68. Yankelevitch-Yahav R, Franko M, Huly A. & Doron R. The Forced Swim Test as a Model of Depressive-like Behavior. Journal of Visualized Experiments : JoVE, 52587, (2015).
69. Jones CK, Peters SC & Shannon HE Efficacy of Duloxetine, a Potent and Balanced Serotonergic and Noradrenergic Reuptake Inhibitor, in Inflammatory and Acute Pain Models in Rodents. Journal of Pharmacology and Experimental Therapeutics 312, 726–732, (2005).
70. Sorensen JB, Nagy G, Varoqueaux F, Nehring RB, Brose N, Wilson MC & Neher E. Differential control of the releasable vesicle pools by SNAP-25 splice variants and SNAP-23. Cell 114, 75–86 (2003). [PubMed: 12859899]
71. Fang Q, Berberian K, Gong L-W, Hafez I, Sørensen JB & Lindau M. The role of the C terminus of the SNARE protein SNAP-25 in fusion pore opening and a model for fusion pore mechanics. Proceedings of the National Academy of Sciences 105, 15388–15392, (2008).
72. Bao H, Das D, Courtney NA, Jiang Y, Briguglio JS, Lou X, Roston D, Cui Q, Chanda B. & Chapman ER Dynamics and number of trans-SNARE complexes determine nascent fusion pore properties. Nature 554, 260, (2018). [PubMed: 29420480]

73. Photowala H, Blackmer T, Schwartz E, Hamm HE, and Alford S. G protein bg-subunits activated by serotonin mediate presynaptic inhibition by regulating vesicle fusion properties. Proc Natl Acad Sci U S A 103, 4281–4286 (2006). [PubMed: 16537522]
74. Zhao A, Ohara-Imaizumi M, Brissova M, Benninger RKP, Xu Y, Hao Y, Abramowitz J, Boulay G, Powers AC, Piston D, Jiang M, Nagamatsu S, Birnbaumer L. & Gu G. Gαo Represses Insulin Secretion by Reducing Vesicular Docking in Pancreatic β-Cells. Diabetes 59, 2522–2529 (2010). [PubMed: 20622165]
75. Fang Q, Zhao Y, Herbst AD, Kim BN & Lindau M. Positively Charged Amino Acids at the SNAP-25 C Terminus Determine Fusion Rates, Fusion Pore Properties, and Energetics of Tight SNARE Complex Zippering. The Journal of Neuroscience 35, 3230–3239, (2015). [PubMed: 25698757]
76. Schwartz EJ, Blackmer T, Gerachshenko T. & Alford S. Presynaptic G-Protein-Coupled Receptors Regulate Synaptic Cleft Glutamate via Transient Vesicle Fusion. The Journal of Neuroscience 27, 5857–5868, (2007). [PubMed: 17537956]
77. Gilsbach R. & Hein L. Are the pharmacology and physiology of α_2 adrenoceptors determined by α2-heteroreceptors and autoreceptors respectively? British Journal of Pharmacology 165, 90. [PubMed: 21658028]
78. Gilsbach R, Röser C, Beetz N, Brede M, Hadamek K, Haubold M, Leemhuis J, Philipp M, Schneider J, Urbanski M, Szabo B, Weinshenker D. & Hein L. Genetic Dissection of α_2 Adrenoceptor Functions in Adrenergic versus Nonadrenergic Cells. Molecular Pharmacology 75, 1160–1170, (2009). [PubMed: 19251826]
79. Banihashemi L. & Rinaman L. Noradrenergic Inputs to the Bed Nucleus of the Stria Terminalis and Paraventricular Nucleus of the Hypothalamus Underlie Hypothalamic–Pituitary–Adrenal Axis But Not Hypophagic or Conditioned Avoidance Responses to Systemic Yohimbine. The Journal of Neuroscience 26, 11442 (2006). [PubMed: 17079674]
80. Freeman ZT, Rice KA, Soto PL, Pate KAM, Weed MR, Ator NA, DeLeon IG, Wong DF, Zhou Y, Mankowski JL, Zink MC, Adams RJ & Hutchinson EK Neurocognitive dysfunction and pharmacological intervention using guanfacine in a rhesus macaque model of self-injurious behavior. Translational Psychiatry 5, e567, (2015).
81. Mineur YS, Bentham MP, Zhou W-L, Plantenga ME, McKee SA & Picciotto MR Antidepressant-like effects of guanfacine and sex-specific differences in c-fos immunoreactivity and paired-pulse ratio in male and female mice. Psychopharmacology 232, 3539–3549, (2015). [PubMed: 26146014]
82. Mantsch JR, Weyer A, Vranjkovic O, Beyer CE, Baker DA & Caretta H. Involvement of Noradrenergic Neurotransmission in the Stress- but not Cocaine-Induced Reinstatement of Extinguished Cocaine-Induced Conditioned Place Preference in Mice: Role for β−2 Adrenergic Receptors. Neuropsychopharmacology 35, 2165–2178, (2010). [PubMed: 20613718]
83. Rasmussen DD, Alexander L, Malone J, Federoff D. & Froehlich JC THE α(2)-ADRENERGIC RECEPTOR AGONIST, CLONIDINE, REDUCES ALCOHOL DRINKING IN ALCOHOL-PREFERRING (P) RATS. Alcohol (Fayetteville, N.Y.) 48, 543–549, (2014).
84. Erb S, Hitchcott PK, Rajabi H, Mueller D, Shaham Y. & Stewart J. Alpha-2 Adrenergic Receptor Agonists Block Stress-Induced Reinstatement of Cocaine Seeking. Neuropsychopharmacology 23, 138, (2000). [PubMed: 10882840]
85. Michaeli A. & Yaka R. Dopamine inhibits GABAA currents in ventral tegmental area dopamine neurons via activation of presynaptic G-protein coupled inwardly-rectifying potassium channels. Neuroscience 165, 1159–1169, (2010). [PubMed: 19944748]
86. Ladera C, Del Carmen Godino M, Cabañero MJ, Torres M, Watanabe M, Luján R. & Sánchez-Prieto J. Pre-synaptic GABAB receptors inhibit glutamate release through GIRK channels in rat cerebral cortex. Journal of Neurochemistry 107, 1506–1517 (2008). [PubMed: 19094055]
87. Johansson JU, Ericsson J, Janson J, Beraki S, Stanić D, Mandic SA, Wikström MA, Hökfelt T, Ögren SO, Rozell B, Berggren P-O & Bark C. An Ancient Duplication of Exon 5 in the Snap25 Gene Is Required for Complex Neuronal Development/Function. PLOS Genetics 4, e1000278, (2008).
88. Jeans AF, Oliver PL, Johnson R, Capogna M, Vikman J, Molnár Z, Babbs A, Partridge CJ, Salehi A, Bengtsson M, Eliasson L, Rorsman P. & Davies KE A dominant mutation in Snap25 causes

impaired vesicle trafficking, sensorimotor gating, and ataxia in the blind-drunk mouse. Proceedings of the National Academy of Sciences 104, 2431–2436, (2007).

89. Schwartz EJ, Gerachshenko T. & Alford S. 5-HT prolongs ventral root bursting via presynaptic inhibition of synaptic activity during fictive locomotion in lamprey. J Neurophysiol 93, 980–988 (2005). [PubMed: 15456802]
90. Chapman ER, Desai RC, Davis AF & Tornehl CK Delineation of the Oligomerization, AP-2 Binding, and Synprint Binding Region of the C2B Domain of Synaptotagmin. Journal of Biological Chemistry 273, 32966–32972, (1998).
91. Chicka MC, Hui E, Liu H. & Chapman ER Synaptotagmin arrests the SNARE complex before triggering fast, efficient membrane fusion in response to Ca2+. Nat Struct Mol Biol 15, 827–835, (2008). [PubMed: 18622390]
92. Cong L, Ran FA, Cox D, Lin S, Barretto R, Habib N, Hsu PD, Wu X, Jiang W, Marraffini LA & Zhang F. Multiplex Genome Engineering Using CRISPR/Cas Systems. Science 339, 819 (2013). [PubMed: 23287718]
93. Yim YY, McDonald WH, Hyde K, Cruz-Rodríguez O, Tesmer JJG & Hamm HE Quantitative Multiple-Reaction Monitoring Proteomic Analysis of Gβ and Gγ Subunits in C57Bl6/J Brain Synaptosomes. Biochemistry 56, 5405–5416, (2017). [PubMed: 28880079]
94. Mazzoni MR, Malinski JA & Hamm HE Structural analysis of rod GTP-binding protein, Gt. limited proteolytic digestion pattern of Gt with four proteases defines monoclonal antibody epitope. J Biol Chem 266, 14072–14081 (1991). [PubMed: 1713215]
95. Schindelin J, Arganda-Carreras I, Frise E, Kaynig V, Longair M, Pietzsch T, Preibisch S, Rueden C, Saalfeld S, Schmid B, Tinevez J-Y, White DJ, Hartenstein V, Eliceiri K, Tomancak P. & Cardona A. Fiji: an open-source platform for biological-image analysis. Nat Meth 9, 676–682, (2012).
96. Schindelin J, Rueden CT, Hiner MC & Eliceiri KW The ImageJ ecosystem: An open platform for biomedical image analysis. Molecular Reproduction and Development 82, 518–529, (2015). [PubMed: 26153368]
97. Byun NE, Grannan M, Bubser M, Barry RL, Thompson A, Rosanelli J, Gowrishankar R, Kelm ND, Damon S, Bridges TM, Melancon BJ, Tarr JC, Brogan JT, Avison MJ, Deutch AY, Wess J, Wood MR, Lindsley CW, Gore JC, Conn PJ & Jones CK Antipsychotic Drug-Like Effects of the Selective M(4) Muscarinic Acetylcholine Receptor Positive Allosteric Modulator VU0152100. Neuropsychopharmacology 39, 1578–1593, (2014). [PubMed: 24442096]
98. Korpi ER, Koikkalainen P, Vekovischeva OY, Mäkelä R, Kleinz R, Uusi-Oukari M. & Wisden W. Cerebellar granule-cell-specific GABAA receptors attenuate benzodiazepine-induced ataxia: evidence from α6-subunit-deficient mice. European Journal of Neuroscience 11, 233–240,(1999).
99. Phillips GR, Huang JK, Wang Y, Tanaka H, Shapiro L, Zhang W, Shan W-S, Arndt K, Frank M, Gordon RE, Gawinowicz MA, Zhao Y. & Colman DR The Presynaptic Particle Web: Ultrastructure, Composition, Dissolution, and Reconstitution. Neuron 32, 63–77,(2001). [PubMed: 11604139]
100. Betke KM, Rose KL, Friedman DB, Baucum AJ, Hyde K, Schey KL & Hamm HE Differential Localization of G Protein βγ Subunits. Biochemistry 53, 2329–2343, (2014). [PubMed: 24568373]
101. Tatarczyńska E, Kłodzińska A, Stachowicz K. & Chojnacka-Wójcik E. Effects of a selective 5-HT1B receptor agonist and antagonists in animal models of anxiety and depression. Behavioural Pharmacology 15, 523–534 (2004) [PubMed: 15577451]
102. Briley M. & Moret C. The importance of norephinephrine in depression. Neuropsychiatric Disease and Treatment 7 (9–13) (2011)
103. Klimek V, Stockmeier C, Overholser J, Meltzer HY, Kalka S, Dilley G. & Ordway GA Reduced Levels of Norepinephrine Transporters in the Locus Coeruleus in Major Depression. Journal of Neuroscience 17 8451–8458 (1997) [PubMed: 9334417]
104. Shamm NL, McDonald MP & Limbird LE The α_{2A}-AR Plays a major protective role in mouse behavioral models of Depression and Anxiety. Journal of Neuroscience 21 4875–4882. (2001) [PubMed: 11425914]

105. Tiger M, Varnas K. Okubo Y. & Lundberg J. The 5HT1B-a potential target for antidepressant treatment. Psychopharmacology 235 1317–1334. (2018) [PubMed: 29546551]

106. Millan MJ, Bervoets K, Rivet JM, Widdowson P, Renouard A, Le Marouille-Girardon S. & Gobert, A. Multiple alpha-2 adrenergic receptor subtypes. II. Evidence for a role of rat R alpha-2A adrenergic receptors in the control of nociception, motor behavior and hippocampal synthesis of noradrenaline. J Pharmacol Exp Ther 270 958–972. (1994) [PubMed: 7932208]

107. Kayser VI, Elfassi IE, Aubel B, Melfort M, Julius D, Gingrich JA, Hamon M, Bourgoin S. Mechanical, thermal and formalin-induced nociception is differentially altered in 5-HT1A−/−, 5-HT1B−/−, 5-HT2A−/−, 5-HT3A−/− and 5-HTT−/− knock-out male mice. Pain 130 235–248 (2007) [PubMed: 17250964]

108. Bannister K. and Dickenson AH What do monoamines do in pain modulation? Curr Opin Support Palliat Care 10 143–148 (2016) [PubMed: 27043287]

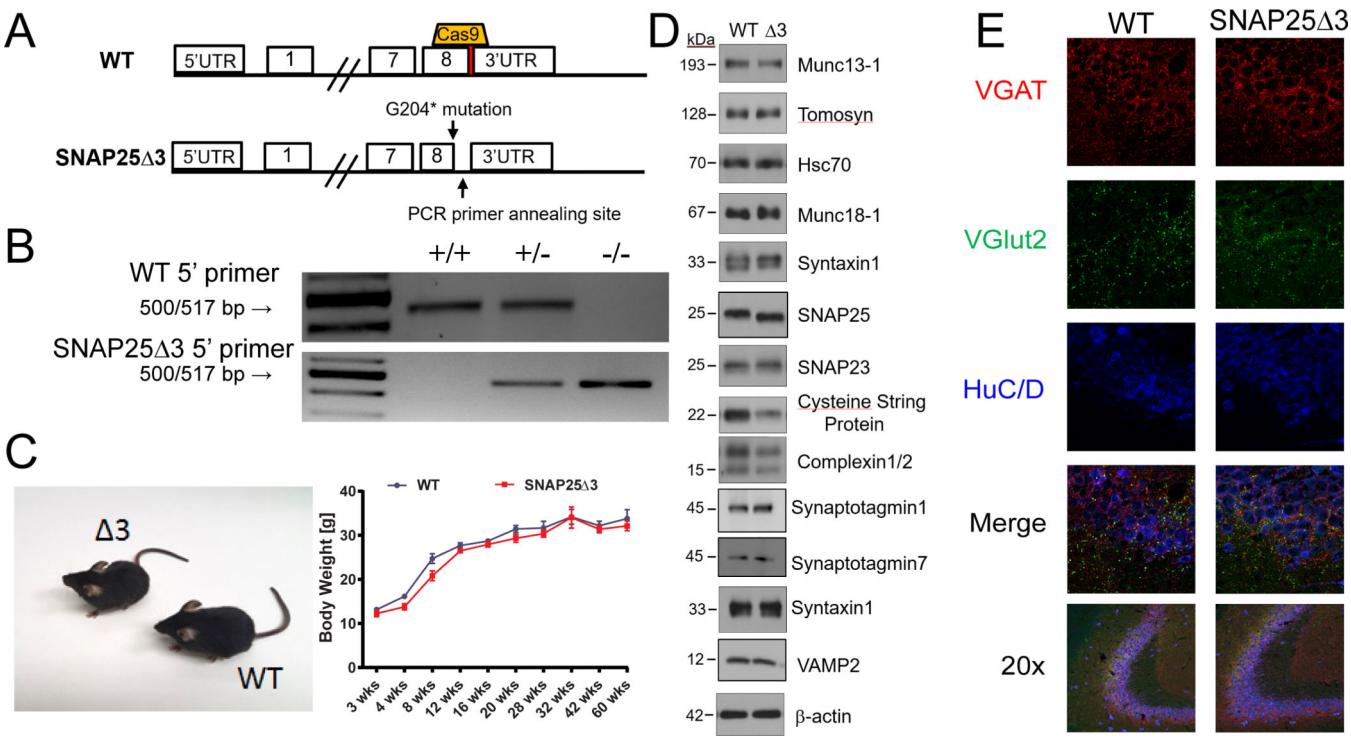

Fig. 1. Generation of the SNAP25Δ3 mouse by CRISPR-Cas9.

(**A**) Graphical representation of the region on mouse chromosome 2 targeted by the sgRNA (top) cloned into px330 and the subsequent region after homology-directed repair (bottom) containing the G204* mutation and cloning site. (**B**) Agarose gel electrophoresis of PCR products generated from reactions containing two different 5' primers used to genotype WT, heterozygote, and homozygote SNAP25Δ3 littermate animals. The WT 5' primer corresponds to the WT region on mouse chromosome 2, whereas the SNAP25Δ3 primer corresponds to the region containing the G204* mutation. (**C**) Gross morphology of WT and SNAP25Δ3 homozygotes (left) and growth curves (right) showing the increase in body mass in WT mice (n = 12 to 18 mice) and SNAP25Δ3 homozygotes (n = 12 to 21 mice) over the first 60 weeks of life of several noncontinuous cohorts. (**D**) Western blotting analysis of presynaptic proteins found within synaptosomal (93,99, 100) fractions (all except for syt I and VII, and VAMP2) or whole mouse brain lysate (syt I and VII, and VAMP2) of WT and SNAP25Δ3 (Δ3) mice. n= 3 to 12 biological replicates per condition. The abundance of cysteine string protein (CSP) in the presynaptic fraction of SNAP25Δ3 synaptosomes was reduced compared to that in WT synaptosomes (see Supplemental Figure 1). No statistically significant difference was found in any of the other proteins. (**E**) Immunofluorescence imaging of GABAergic (VGAT) and glutamatergic (vGlut2) immunoreactive appositions(46) within hippocampal slices taken from adult WT or SNAP25Δ3 homozygotes. Data are representative of four mice per genotype. HuC/D was used as a pan-neuronal marker.

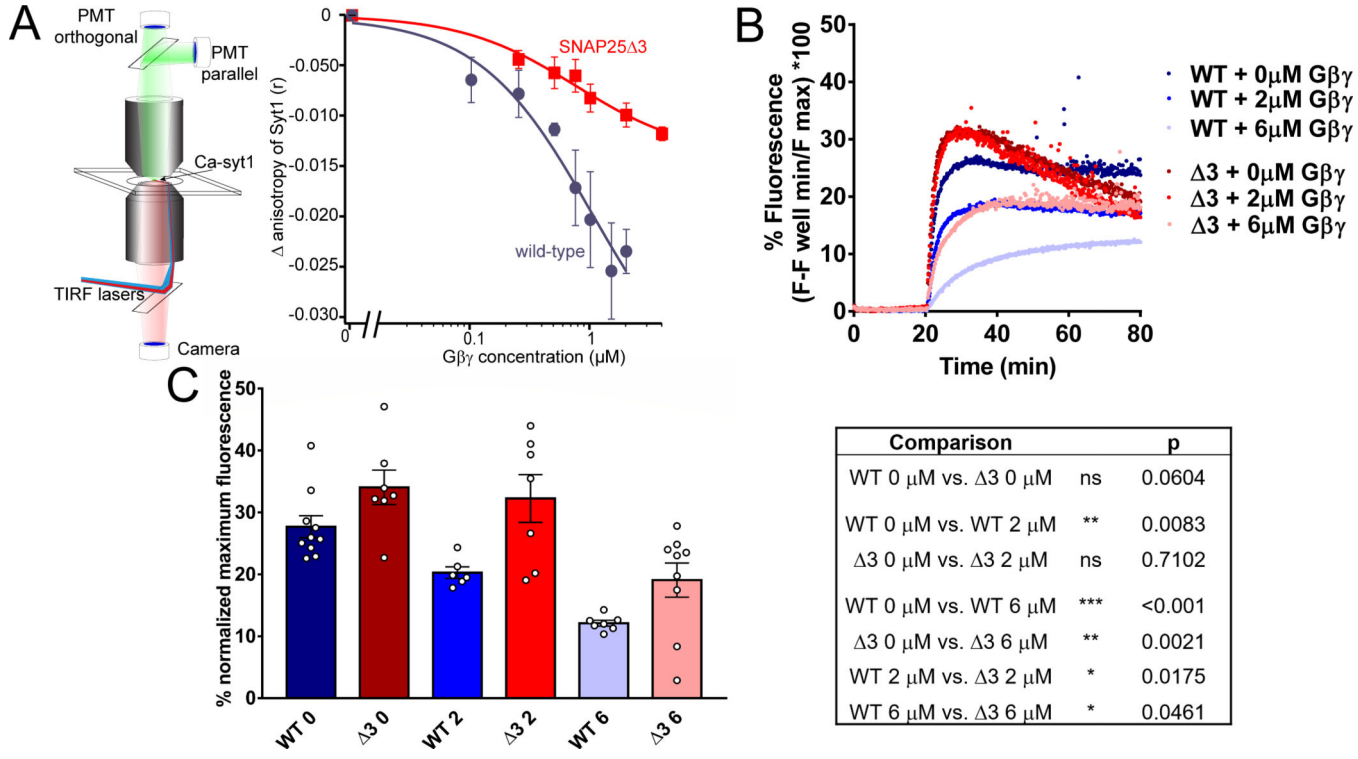

Comparison		p
WT 0 μM vs. Δ3 0 μM	ns	0.0604
WT 0 μM vs. WT 2 μM	**	0.0083
Δ3 0 μM vs. Δ3 2 μM	ns	0.7102
WT 0 μM vs. WT 6 μM	***	<0.001
Δ3 0 μM vs. Δ3 6 μM	**	0.0021
WT 2 μM vs. Δ3 2 μM	*	0.0175
WT 6 μM vs. Δ3 6 μM	*	0.0461

Figure 2. SNAP25Δ3 impairs Gβγ competition with synaptotagmin I and inhibition of calcium-synaptotagmin I-mediated liposome fusion.

A. Syt1 competition with Gβγ at t-SNARE complexes in lipid bilayers. Left panel: Schematic of the imaging system. A lipid bilayer consisting of 55% PC/15%PE/29%PS/1% DiD harboring t-SNARE complexes was fused to a glass coverslip and imaged using TIRF illumination from a 1.45 NA 60x lens through a laser TIRF illuminator. 1 μM Ca-AF-syt1 was applied over the bilayer (100 μM Ca^{2+}). Graph shows $G\beta_1\gamma_1$ concentration dependence of the change in anisotropy produced by AF-syt I binding to WT (blue) or SNAP25Δ3 (red)-containing t-SNAREs embedded in the lipid membranes. The ability of $G\beta_1\gamma_1$ to displace AF-syt1 from SNAP25Δ3 t-SNAREs was reduced to 47±13% of its displacement of AF-syt1 from WT SNAP-25, as measured by change in anisotropy (n = 5 biological replicates per group, p = 0.019). AF-sytI displacement from WT t-SNAREs had an IC_{50} of 502 nM (95% CI: 150nM). **B.** Traces of lipid mixing experiments in which liposomes containing t-SNARE complexes made with SNAP25WT or SNAP25Δ3 were incubated with liposomes containing VAMP2 and a FRET pair of NBD-PE and rhodamine-PE in addition to 10μM sytI and $G\beta_1\gamma_1$. At t= 20 min, 1mM $CaCl_2$ was added. **C.** Left panel: Bar graph of maximum fluorescence values: 2μM Gβγ significantly inhibits lipid mixing with liposomes containing t-SNAREs made with SNAP25WT (p=0.0083) but not SNAP25Δ3 (p = 0.71), while 6μM Gβγ inhibits significantly less in SNAP25Δ3 liposomes than SNAP25WT (p = 0.0461). Right panel: Table of significance values for lipid mixing experiments (Student's two-tailed t-test). Experiments were repeated 6–8 times for 6–10 technical replicates.

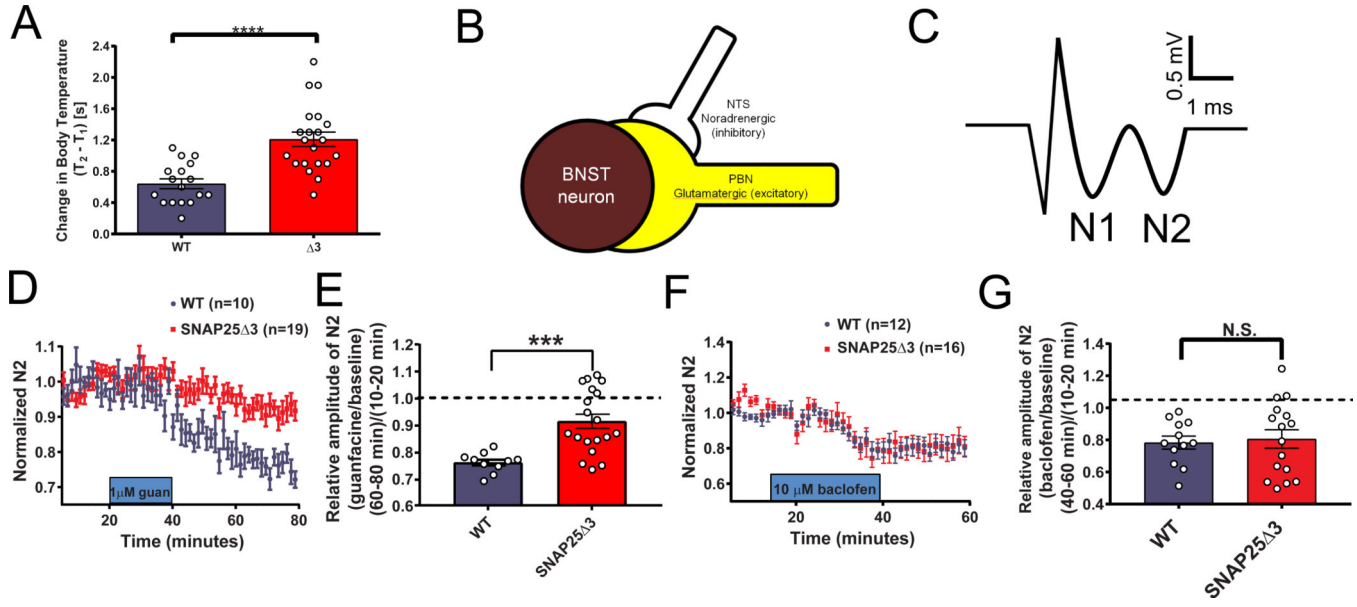

Figure 3. SNAP25Δ3 mice have altered stress responses and impaired α_{2a} heteroreceptor signaling in the BNST.

A. Bar graph of significant changes in rectal temperature subsequent to handling in singly-housed littermate male WT (n=17 mice) and SNAP25Δ3 homozygotes (n=21 mice) of 13–14 weeks of age (****p<0.00001). **B.** Diagram showing synaptology of α_{2a} heteroreceptor inhibitory signaling on excitatory parabrachial inputs on the bed nuclei of the stria terminalis. **C.** Example field potential from coronal brain slices containing the dorsal BNST illustrating the N1 and N2 downward deflections. **D.** Normalized change in the N2 component of excitatory postsynaptic potentials recorded in the BNST-containing slices taken from WT (in blue) and SNAP25Δ3 homozygote male mice (in red) at an age of >8 weeks. 1uM guanfacine was administered from t= 20 min to t= 40 min. **E.** Bar graph showing relative amplitude of the N2 component of EPSPs at t= 80 min as a fraction of the amplitude prior to the administration of guanfacine at t=10–20min. Guanfacine reduced the N2 component of the EPSP significantly less in slices from SNAP25Δ3 homozygotes than WT (***p < 0.001, Mann-Whitney u-test). WT: n=10 slices from 7 mice. SNAP25Δ3: n= 19 slices from 10 mice. **F.** Normalized change in the N2 component of excitatory postsynaptic potentials recorded in the BNST-containing slices taken from WT and SNAP25Δ3 homozygotes at an age of 8–14 weeks. 10uM baclofen was administered from t=20 min to t=40 min. **G.** Bar graph showing relative amplitude of the N2 component of EPSPs at t= 80 min as a fraction of the amplitude prior to the administration of baclofen at t= 10– 20min. No significant differences were observed between genotypes(p = 0.92). WT: n=12 slices from 4 mice. SNAP25Δ3: n = 16 slices from 5 mice.

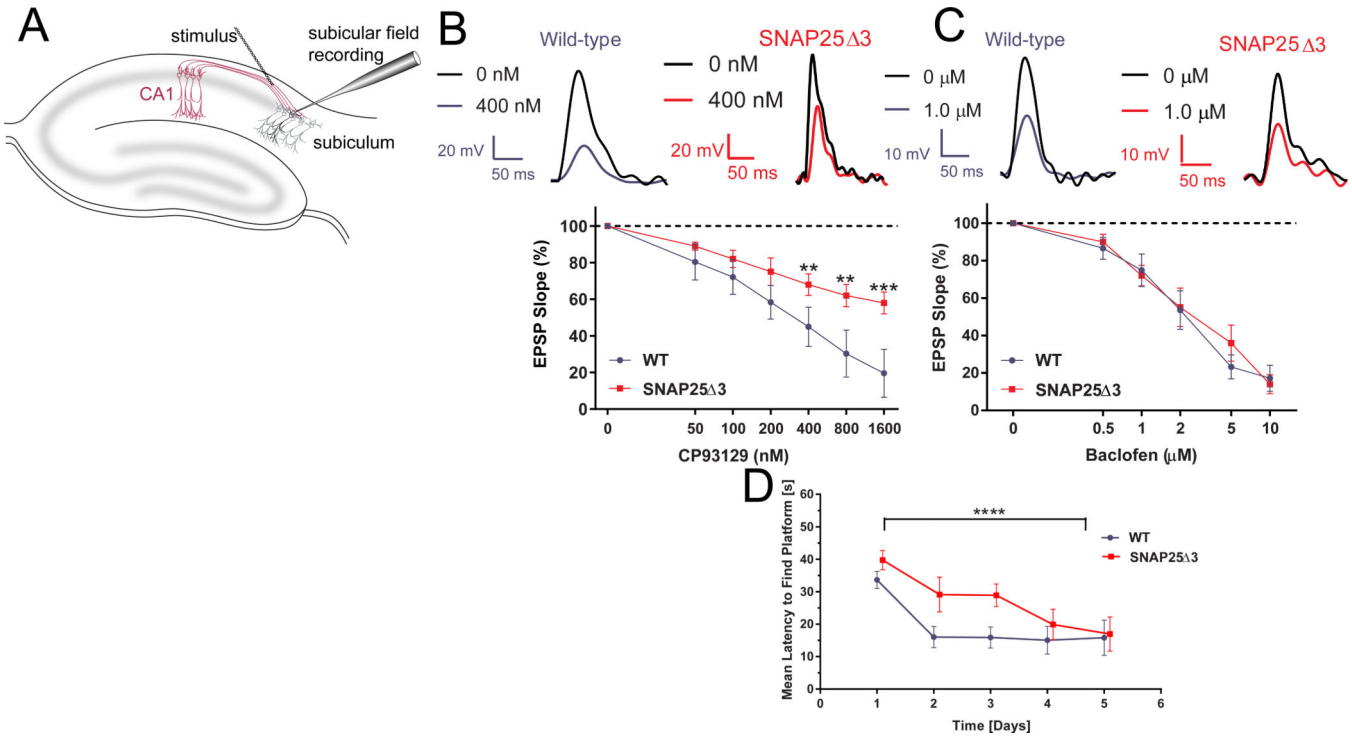

Figure 4. SNAP25Δ3 homozygotes have impaired $G_{i/o}$-coupled GPCR signaling in CA1/subiculuar hippocampal neurons and show impaired hippocampal spatial learning.

A. Diagram of the hippocampal field recording paradigm. Stimulation with bipolar electrodes over the CA1-subicular pathway evoked field EPSPs recorded in basal dendrites of subicular pyramidal neurons in AP5 (50 μM) and bicuculline (5μM) to isolate AMPAR-mediated responses. **B.** Traces from CA1-subicular recordings in WT (left panel) and SNAP25Δ3 (right panel) slices at 0 and 400 nM CP93129. Bottom panel: Dose response of the effect of CP93129 on the AMPA component of these field EPSPs from 6-week old littermate WT (in blue) or SNAP25Δ3 homozygotes (in red). Amplitudes were normalized to the control response. CP93129 was significantly more potent in WT than SNAP25Δ3 (**p = 0.0068, 400 nM; **p = 0.0035, 800 nM; ***p = 0.001, 1600 nM; Student's t-test). WT: n= 8 slices from 6 mice. SNAP25Δ3: n= 5 slices from 5 mice. **C.** Traces from field recordings in wild-type (left panel) and SNAP25Δ3 (right panel) slices at 0 and 1.0 μM baclofen. Bottom panel: Dose-response of the effect of baclofen on field EPSPs recorded in the WT or SNAP25Δ3 hippocampal slices. No significant differences were detected by genotype. WT and SNAP25Δ3: n= 5 slices from 5 mice for both genotypes. **D.** Comparison between age-matched littermate WT and SNAP25Δ3 homozygotes in the acquisition of the Morris Water Maze Task over a 5 day trial period by genotype ($p<0.05$) and time ($p<0.0001$). n=11 WT mice and 11 SNAP25Δ3 mice.

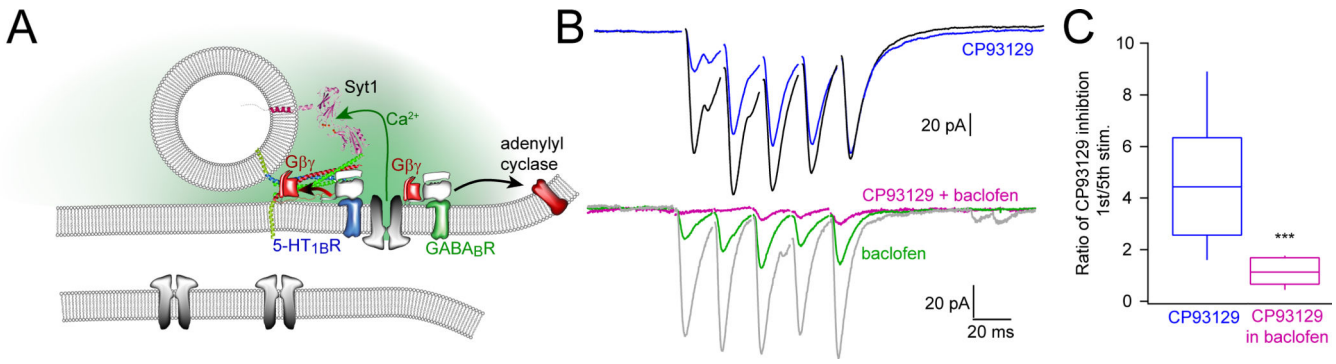

Figure 5. Synergy between 5-HT$_{1B}$ and GABA$_B$ at the CA1/subicular synapse.

A. Schematic of targets within the presynaptic terminal for $G_{i/o}$-coupled GPCRs. In CA1 terminals, 5-HT$_{1b}$Rs release Gβγ to bind SNAREs and GABA$_B$ receptors release Gβγ to inhibit Ca^{2+} channels. Synergistic effects of 5-HT$_{1b}$Rs and GABA$_B$R$_s$. **B**. Stimulation of the CA1-subicular pathway evoked whole cell recorded EPSCs in subicular pyramidal neurons. During repetitive stimulation, CP93129 (400 nM, blue) substantially inhibited the first response, but response amplitudes recovered during the stimulus train. The ratio of inhibition of the 1st vs. the 5th response was 4.6±0.8. Baclofen (1 μM, green) uniformly inhibited EPSCs throughout the stimulus train; the ratio was 1.1±0.2. Addition of CP93129 + baclofen, pink) substantially inhibited responses throughout the stimulus train (***p=0.0002). WT: n= 8 slices from 6 mice. SNAP25Δ3: n= 5 slices from 5 mice. **C.** Quantitation of the effects of CP93129 (400 nM) alone and after addition of baclofen.

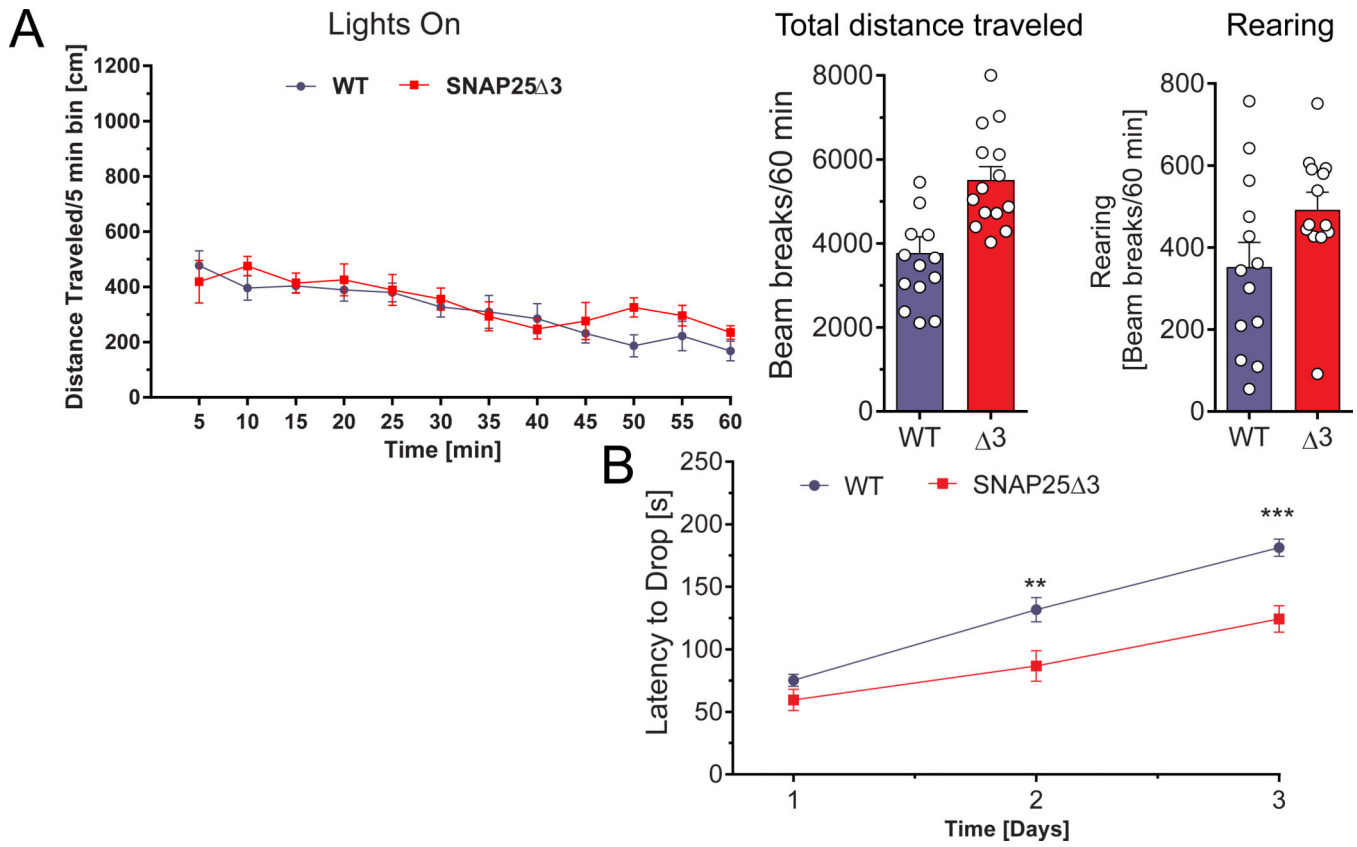

Figure 6. SNAP25Δ3 mutant mice have impaired motor coordination and altered gait.

A. Left panel: Mutant mice have normal locomotor behavior in the open chamber. Plot of distance traveled in five-minute intervals in a brightly illuminated open field for 15 week old littermate SNAP25Δ3 homozygotes (red line) (n=14 mice) and WT (blue line) (n= 15 mice). Middle and right panels: Total distance traveled (p=0.8088) and number of rearing movements (p=0.0796) made are plotted below for each genotype. **B**. Plot of latency to drop from an accelerating, rotating beam for 16 week old male WT (n=15 mice) and homozygotes SNAP25Δ3 (n=14 mice) in the rotarod paradigm. Animals were tested daily for three consecutive days. Age-matched littermate SNAP25Δ3 homozygotes had a significantly reduced latency to drop on the second and third day of testing compared to wild-type controls (**, $p<0.01$, ***, $p<0.001$, Student's two-tailed t-test).

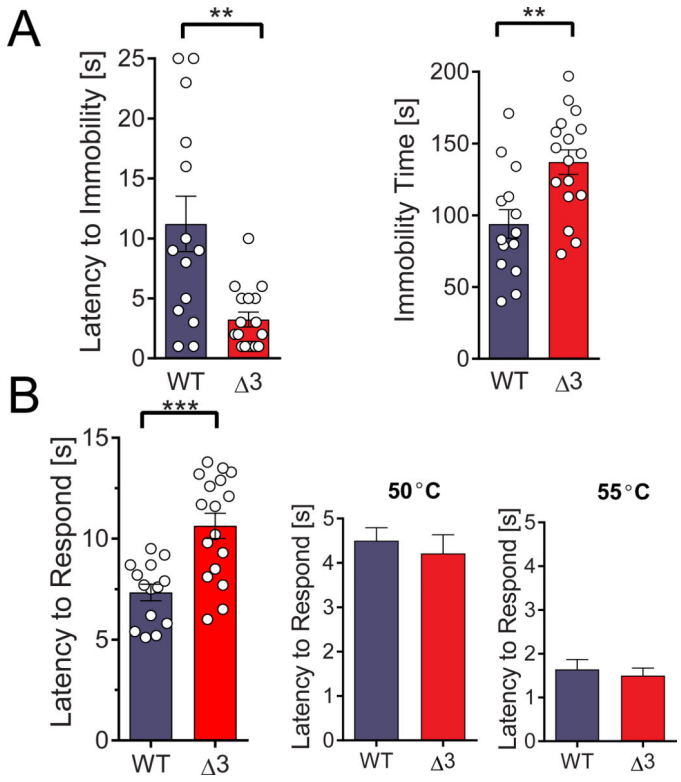

Figure 7. SNAP25Δ3 mutant mice showed altered affect and supraspinal nociception.

A. SNAP25Δ3 animals show greater immobility in the forced swim paradigm. Left panel: Bar graph shows the time spent immobile subsequent to immersion for 16–17-week old littermate male WT or SNAP25Δ3 homozygotes. Immobility time was significantly greater for SNAP25Δ3 than WT littermates (**p< 0.01, Student's two-tailed t-test) Right panel: Bar graph showing the latency to immobility subsequent to immersion for littermate male WT or SNAP25Δ3 homozygotes in the forced swim paradigm. Latency time before immobility was significantly lower for SNAP25Δ3 than WT littermates (**p< 0.01). **B.** SNAP25Δ3 animals have impaired nociception. Left panel: Bar graph showing latency required for 20 week old littermate male WT or SNAP25Δ3 homozygotes to respond to supraspinal thermal pain in the hot plate paradigm, in which animals are placed on a plate heated to 55°C and the time required to produce a paw movement is measured. Latency time was significantly greater for SNAP25Δ3 than WT littermates (**p< 0.01, Student's two-tailed t-test). Right panel: Bar graph showing latency required for 21-week old littermate male WT or SNAP25Δ3 homozygotes to respond to spinal thermal nociception in in the tail flick paradigm, in which mouse tails are immersed in a hot water bath heated to 50° or 55° C and the time required for tail movement is recorded. No differences were detected between littermate SNAP25Δ3 and WT (p= 0.29 and 0.53 respectively, Student's two-tailed t-test). For A and B, 14 WT mice and 17 SNAP25Δ3 homozygotes were used.